

# AEGIS: THE CLUSTERING OF X-RAY AGN RELATIVE TO GALAXIES AT $Z \sim 1$

ALISON L. COIL<sup>1,2,3</sup>, ANTONIS GEORGAKAKIS<sup>4,5</sup>, JEFFREY A. NEWMAN<sup>6</sup>, MICHAEL C. COOPER<sup>2</sup>, DARREN CROTON<sup>7</sup>, MARC DAVIS<sup>8</sup>, DAVID C. KOO<sup>9</sup>, E.S. LAIRD<sup>4</sup>, K. NANDRA<sup>4</sup>, BENJAMIN J. WEINER<sup>2</sup>, CHRISTOPHER N. A. WILLMER<sup>2</sup>, RENBIN YAN<sup>10</sup>,

*Draft version February 3, 2022*

## ABSTRACT

We measure the clustering of non-quasar X-ray AGN at  $z = 0.7 - 1.4$  in the AEGIS field. Using the cross-correlation of 113 *Chandra*-selected AGN, with a median  $\log L_X = 42.8 \text{ erg s}^{-1}$ , with  $\sim 5,000$  DEEP2 galaxies, we find that the X-ray AGN are fit by a power law with a clustering scale length of  $r_0 = 5.95 \pm 0.90 h^{-1} \text{ Mpc}$  and slope  $\gamma = 1.66 \pm 0.22$ . X-ray AGN have a similar clustering amplitude as red, quiescent and ‘green’ transition galaxies at  $z \sim 1$  and are significantly more clustered than blue, star-forming galaxies. The X-ray AGN clustering strength is primarily determined by the host galaxy color; AGN in red host galaxies are significantly more clustered than AGN in blue host galaxies, with a relative bias that is similar to that of red to blue DEEP2 galaxies. We detect no dependence of clustering on optical brightness, X-ray luminosity, or hardness ratio within the ranges probed here. We find evidence for galaxies hosting X-ray AGN to be more clustered than a sample of galaxies with matching joint optical color and magnitude distributions. This implies that galaxies hosting X-ray AGN are more likely to reside in groups and more massive dark matter halos than galaxies of the same color and luminosity without an X-ray AGN. In comparison to optically-selected quasars in the DEEP2 fields, we find that X-ray AGN at  $z \sim 1$  are more clustered than optically-selected quasars (with a  $2.6\sigma$  significance) and therefore may reside in more massive dark matter halos. Our results are consistent with galaxies undergoing a quasar phase while in the blue cloud before settling on the red sequence with a lower-luminosity X-ray AGN, *if* they are similar objects at different evolutionary stages.

*Subject headings:* cosmology: large-scale structure of the universe — galaxies: active — galaxies: high-redshift — X-rays: galaxies

## 1. INTRODUCTION

It has recently become clear that black holes play a key role in the evolution of galaxies. It is now understood that most galaxies have supermassive black holes in their nuclei (for reviews, see e.g. Richstone et al. 1998; Ferrarese & Ford 2005) and that these black holes power active galactic nuclei (AGN). There are strong observed correlations between black hole mass and galaxy properties such as the stellar velocity dispersion in the bulge (Gebhardt et al. 2000; Ferrarese & Merritt 2000), that indicate some form of feedback or connection between the growth of black holes and their parent galaxies.

It remains unclear how galaxies and AGN co-evolve and what impact the AGN have on the evolution of their host galaxies. It is also not known what the accretion

mechanism is for AGN and what their fueling source is. Measuring the environments and clustering properties of AGN is key to understanding their nature: constraining how they are triggered and fueled, inferring their lifetimes, and determining which galaxy populations host different kinds of AGN (quasars, Seyferts, radio-loud AGN, etc.). Additionally, clustering measurements constrain the masses of the dark matter halos which host AGN and allow various types of AGN to be placed in a cosmological context. These pieces are all necessary to understand the relevance of AGN for galaxy evolution.

Cosmological numerical simulations, both hydrodynamic and semi-analytic, predict the co-evolution of black holes and galaxies as well as the lifetimes and fueling mechanisms for AGN. In these simulations the AGN physics itself is not well resolved and often assumptions are made regarding the details of accretion and feedback from the AGN. Most models of high luminosity AGN assume that mergers drive the AGN accretion (e.g., Kauffmann & Haehnelt 2000; Springel, Di Matteo, & Hernquist 2005a), though lower-luminosity AGN may be fueled in other ways (Hopkins & Hernquist 2006). Recent theoretical models often include some form of AGN feedback, motivated by the observational links between the properties of galaxies and their central black holes; this feedback can cause a decline in the star formation activity of massive galaxies, creating red ellipticals. Many models find that AGN feedback of some sort is in fact required to create the red sequence of quiescent galaxies (though see Naab et al. (2007) and Dekel & Birnboim

<sup>1</sup> Hubble Fellow

<sup>2</sup> Steward Observatory, University of Arizona, Tucson, AZ 85721

<sup>3</sup> Department of Physics, University of California, San Diego, CA 92093

<sup>4</sup> Astrophysics Group, Blackett Laboratory, Imperial College, London SW7 2BZ, UK

<sup>5</sup> National Observatory of Athens, V. Paulou & I. Metaxa, 11532, Greece

<sup>6</sup> Department of Physics and Astronomy, University of Pittsburgh, Pittsburgh, PA 15260

<sup>7</sup> Centre for Astrophysics & Supercomputing, Swinburne University of Technology, P.O. Box 218, Hawthorn, VIC 3122, Australia

<sup>8</sup> Department of Astronomy, University of California, Berkeley, CA 94720

<sup>9</sup> University of California Observatories/Lick Observatory, Department of Astronomy and Astrophysics, University of California, Santa Cruz, CA 95064

<sup>10</sup> Department of Astronomy and Astrophysics, University of Toronto, Toronto, ON M5S 3H4, Canada

(2008) for counter examples). For massive galaxies, accretion of gas from cooling flows in dense environments may produce relatively low-luminosity AGN that in turn heat the bulk of the cooling gas and prevent it from falling into the galaxy's center to form stars (e.g., Cattaneo et al. 2006; Croton et al. 2006). Other models propose that mergers trigger quasars that drive outflows that sweep away the gas, not allowing it to form stars (e.g., Springel, Di Matteo, & Hernquist 2005a).

These theoretical models can be tested using observations of the location of AGN within the web of large-scale structure. Measuring the clustering of both low and high luminosity AGN is crucial for determining if their fueling mechanisms differ and searching for links between AGN fueling and local environment. To measure clustering properties accurately requires large samples to overcome both Poisson errors and cosmic variance.

It is now known that optical surveys fail to detect a large fraction of the full AGN population, particularly weak or obscured AGN (e.g., Mushotzky et al. 2000; Alexander et al. 2001; Mushotzky 2004; Brandt & Hasinger 2005). X-ray detection is generally recognized as a more robust way to obtain a relatively unbiased AGN sample, though it does not detect all AGN (e.g., Donley et al. 2005; Heckman et al. 2005), especially optically-varying AGN (Morokuma et al. 2008). As soft X-ray samples can miss obscured AGN (e.g., Comastri & Fiore 2004), an ideal sample includes objects detected in either the hard or soft bands; however, even the deepest of the current X-ray surveys are likely to miss the most heavily obscured “Compton thick” AGN (Gilli, Comastri, & Hasinger 2007).

Most previous attempts to measure the clustering of X-ray AGN in *ROSAT*, *XMM-Newton* and *Chandra* surveys have been fundamentally limited by a lack of spectroscopic redshifts, resulting in conflicting values for the inferred correlation amplitude. Most studies measure the projected angular clustering of X-ray sources (Akylas, Georgantopoulos, & Plionis 2000; Yang et al. 2003; Basilakos et al. 2004; Miyaji et al. 2007; Plionis et al. 2008); to interpret the angular clustering the redshift distribution of the sources,  $dN/dz$ , must be known to fairly high precision, as the inferred correlation length is particularly sensitive to the range of redshifts spanned. Lacking a large sample of spectroscopic redshifts for these sources, most authors assume a redshift distribution using the observed X-ray luminosity function and AGN population synthesis models. However, errors in the  $dN/dz$  distribution are generally not propagated to the inferred correlation length, so that the quoted errors on the clustering amplitude are highly underestimated and often the inferred correlation lengths are extremely large (e.g.,  $r_0 = 9 - 19 h^{-1}$  Mpc in Basilakos et al. (2005)). Additionally, most studies do not include cosmic variance errors, which can be large for the relatively small fields with deep X-ray data.

Recently, several studies have employed spectroscopic redshifts to measure the direct correlation function of X-ray AGN. Mullis et al. (2004) use data from the *ROSAT* North Ecliptic Pole survey to measure the clustering of 219 bright ( $L_x = 9.2 \times 10^{43} h_{70}^{-2} \text{erg s}^{-1}$ ), soft (0.5-2.0 keV) X-ray sources at  $z \sim 0.2$  on large scales,  $r = 5 - 100 h^{-1}$  Mpc, finding a correlation length of  $r_0 = 7.4 \pm 1.9 h^{-1}$  Mpc. Gilli et al. (2005) measure the clustering of

X-ray AGN at  $z = 0 - 4$  in both of the  $\sim 0.1$  sq. degree *Chandra* Deep Fields (CDF), finding  $r_0 = 10.3 \pm 1.7 h^{-1}$  Mpc and  $\gamma = 1.33 \pm 0.14$  for 240 sources in the northern field and  $r_0 = 5.5 \pm 0.6 h^{-1}$  Mpc and  $\gamma = 1.50 \pm 0.12$  for 124 sources in the southern field. These error bars do not include cosmic variance, however, which is severe for the small CDF fields and most likely accounts for the discrepancy between the measurements. Yang et al. (2006) measure the clustering of 233 spectroscopic sources at  $z = 0.1 - 3$  in the 0.4 sq. degree *Chandra* CLASXS area, as well as 252 sources in the CDFN field. They find  $r_0 = 5.7 + 0.8 / - 1.5 h^{-1}$  Mpc in CLASXS and  $r_0 = 4.1 + 0.7 / - 1.1 h^{-1}$  Mpc in the CDFN field, where the errors are from bootstrap resampling of the data. More recently, Gilli et al. (2009) find in the 2 sq. degree XMM-COSMOS field that 349 X-ray AGN with  $0.4 < z < 1.6$  have a clustering scale length of  $r_0 = 5.2 \pm 1.0 h^{-1}$  Mpc and  $\gamma = 1.7 \pm 0.2$ , where the error bars quoted include only Poisson errors.

Ideally, one would like to measure the correlation amplitude of AGN in a relatively narrow redshift range using spectroscopic redshifts, and compare with the clustering of galaxies in the same volume to understand the relationship of AGN to their host galaxies and avoid much of the cosmic variance error. In this paper, we measure the clustering properties of 113 X-ray selected AGN in the redshift range  $0.7 < z < 1.4$  (a subset of the 463 X-ray objects in this field with spectroscopic redshifts) using deep *Chandra* data in the Extended Groth Strip (EGS). For comparison, the only other X-ray field that has a large sample of spectroscopic redshifts and is comparable in both size and depth to the EGS is the XMM-COSMOS field. The environments of 53 X-ray selected AGN in the EGS were measured in Georgakakis et al. (2007) and compared to galaxies in the same volume; they found that X-ray AGN avoid under-dense regions and have environments similar to those of optically red galaxies. Here we measure the clustering of a larger sample of AGN in the same field, as a function of scale, and compare to galaxies in the same volume. To measure the clustering amplitude of the AGN we do not use the auto-correlation function of the AGN, as it is very sensitive to spatially-varying selection functions (which is troublesome given that the *Chandra* point spread function and telescope effective area vary across the field of view) and is subject to large shot noise due to the relatively small AGN sample size. Instead, we take advantage of the large, uniformly selected DEEP2 galaxy survey in the EGS and measure the clustering of more abundant galaxies around the AGN using the two-point cross-correlation function and then divide by the correlation function of the galaxies themselves to determine the AGN clustering strength. We measure the clustering of the AGN on both small ( $< 1 h^{-1}$  Mpc) and large ( $1 - 10 h^{-1}$  Mpc) scales and compare the results to the clustering of galaxies from the DEEP2 galaxy redshift survey as a function of color and luminosity at the same redshift, to understand which galaxies host these AGN and to constrain their host dark matter halo masses. By comparing these clustering measurements with those for optically-selected samples of luminous AGN, we can investigate the relationship between accretion activity and large-scale structure, which strongly constrains theoretical models of the interplay between AGN and galaxy

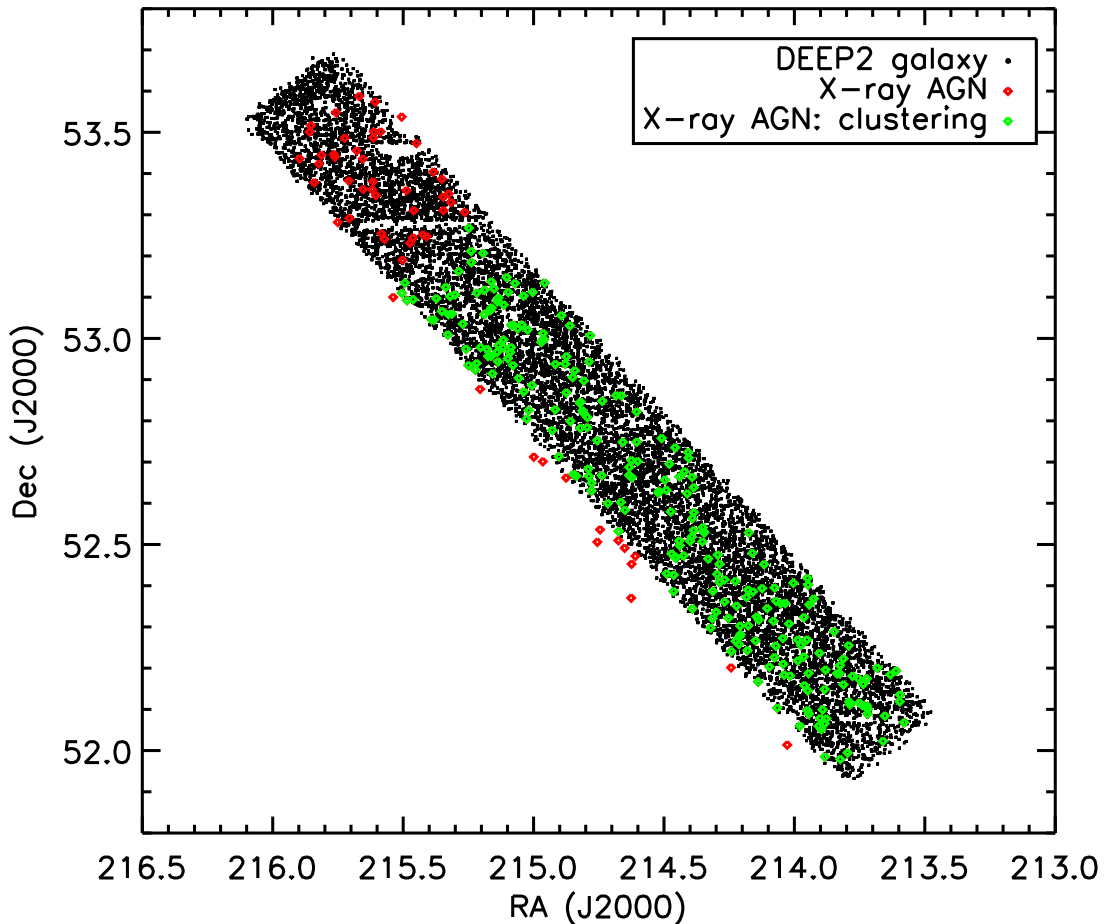


FIG. 1.— Spatial distribution of DEEP2 galaxies (black squares) and X-ray AGN (colored diamonds) with  $0.2 < z < 1.4$  in the Extended Groth Strip field. X-ray AGN used for the clustering analysis performed here are shown in green; these sources are within the boundary of the DEEP2 survey in this field and cover the lower three quadrants of the strip, where the DEEP2 selection function is uniform (see Section 3.2 for details).

evolution.

The outline of the paper is as follows: §2 briefly describes the *Chandra* and DEEP2 surveys in the EGS and presents additional spectroscopic follow-up of X-ray sources taken with the MMT. In §3 we discuss the optical properties of the X-ray AGN and define the various AGN and galaxy samples used here. §4 outlines the methods used to measure the cross-correlation function and infer the real-space auto-correlation function. Results for various AGN and galaxy samples are shown in §5, as a function of optical and X-ray properties. These results are discussed in §6, and we conclude in §7. To convert measured redshifts to comoving distances along the line of sight, we assume a flat  $\Lambda$ CDM cosmology with  $\Omega_m = 0.3$  and  $\Omega_\Lambda = 0.7$ . We define  $h \equiv H_0/(100 \text{ km s}^{-1} \text{ Mpc}^{-1})$  and quote correlation lengths,  $r_0$ , in comoving  $h^{-1} \text{ Mpc}$ .

## 2. DATA

### 2.1. *Chandra* Imaging

X-ray AGN are identified using deep *Chandra* data (Laird et al. 2009) obtained as part of the AEGIS survey of the Extended Groth Strip (EGS, Davis et al. 2007). This dataset consists of 8 *Chandra* ACIS-I pointings, each with a total integration time of about 200 ks split in

at least 3 shorter exposures obtained at different epochs. The data reduction, source detection and flux estimation are described in detail by Laird et al. (2009). In brief, after merging the individual observations into a single event file, images are constructed in four energy bands 0.5–7.0 keV (full), 0.5–2.0 keV (soft), 2.0–7.0 keV (hard) and 4.0–7.0 keV (ultra-hard). The count rates in the above energy intervals are converted to fluxes in the bands 0.5–10, 0.5–2, 2–10 and 5–10 keV, respectively. The limiting flux in each of these bands for a point source is estimated to be  $3.5 \times 10^{-15}$ ,  $1.1 \times 10^{-16}$ ,  $8.2 \times 10^{-16}$ , and  $1.4 \times 10^{-15} \text{ erg s}^{-1} \text{ cm}^{-2}$ , respectively. Sources are not required to be detected in both the soft and hard bands, though most are (for the main AGN sample used here, described in Section 3 below, 29% of the sources are detected in the soft band only and 9% are detected in the hard band only). The X-ray catalog comprises a total of 1325 unique sources over  $0.63 \text{ deg}^2$  to a Poisson detection probability threshold of  $4 \times 10^{-6}$ . We identify optical counterparts of the *Chandra* X-ray sources using the maximum likelihood (LR) method as described in Laird et al. (2009). A total of 895 sources have optical counterparts to  $R_{AB} = 24.1 \text{ mag}$  ( $LR > 0.5$ ).

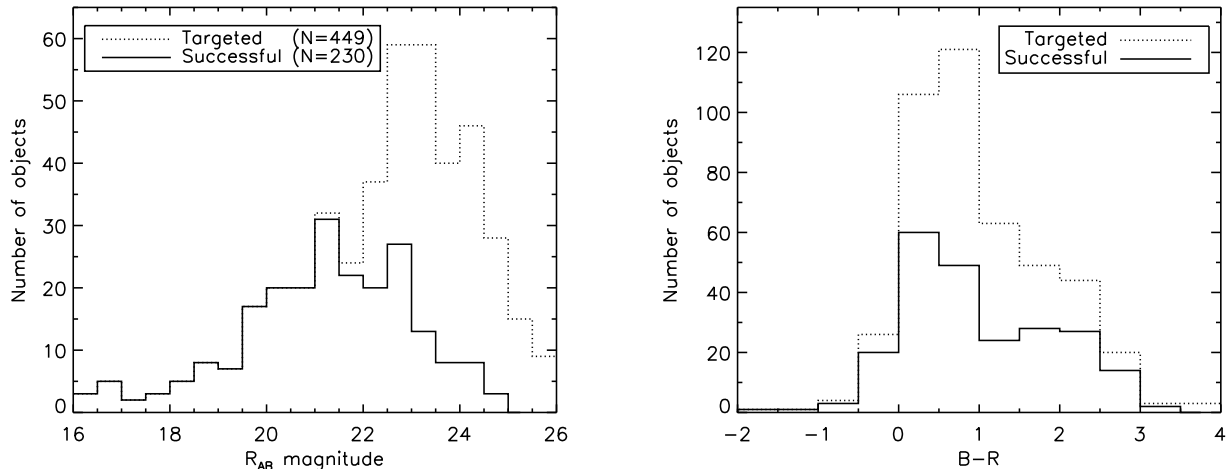


FIG. 2.— Left: Optical  $R_{AB}$  magnitude distribution for X-ray sources targeted (dotted line) for MMT/Hectospec spectroscopic observations. The solid line shows objects which yielded a high-confidence spectroscopic redshift. Right: Optical apparent  $B - R$  colors for X-ray sources targeted (dotted line) and for those with a high-confidence redshift (solid line).

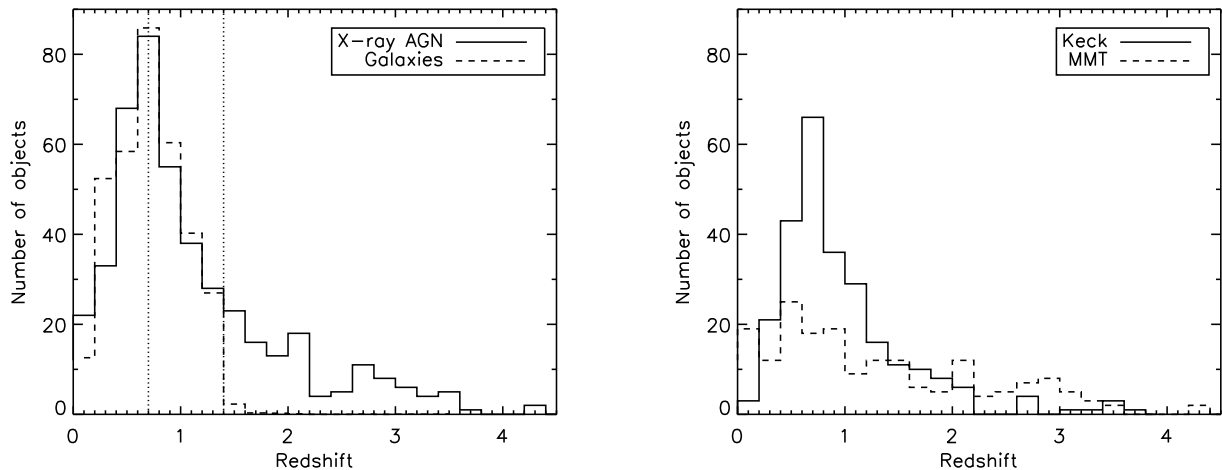


FIG. 3.— Left: Redshift distribution of all 463 *Chandra* X-ray sources in AEGIS with spectroscopic redshifts (solid line) and DEEP2 galaxies in the EGS (dashed line). The dotted vertical lines show the redshift range used here to measure the clustering properties of X-ray AGN and compare with galaxies. Right: The redshift distribution of X-ray sources where the redshift was measured in Keck/DEIMOS spectra (solid line, 233 sources) or MMT/Hectospec spectra (dashed line, 230 sources).

## 2.2. DEEP2 Spectroscopy

Spectroscopic redshifts were obtained for 463 X-ray sources in AEGIS, 233 (50%) of which are from the DEEP2 Galaxy Redshift Survey (Davis et al. 2000, 2003) and 230 (50%) of which were obtained with follow-up spectroscopic observations at the MMT, as described in §2.3. The DEEP2 survey is a completed project using the DEIMOS spectrograph (Faber et al. 2003) on the 10m Keck II telescope to survey optically-selected galaxies at  $z \simeq 1$  in a comoving volume of approximately  $5 \times 10^6 h^{-3} \text{ Mpc}^3$ . Using  $\sim 1$  hour exposure times, the survey has measured high-confidence redshifts for  $> 30,000$  galaxies, most in the redshift range  $0.7 < z < 1.5$ , to a limiting magnitude of  $R_{AB} = 24.1$ . Roughly 65% of the galaxies to  $R_{AB} = 24.1$  were targeted for spectroscopy, and of those targeted, successful redshifts were measured for  $\sim 65\%$ .

One of the DEEP2 fields is the EGS, where the survey has measured  $> 11,000$  high-confidence redshifts

(Davis et al. 2007); unlike other DEEP2 fields, objects with colors indicating that they have  $z < 0.7$  are still observed in the EGS. The DEEP2 spectra have high resolution ( $R \sim 5,000$ ), and rms redshift errors (as determined from repeated observations) are  $< 35 \text{ km s}^{-1}$ . After restricting to  $0.7 < z < 1.4$  and the area covered by the AGN samples described below, the EGS DEEP2 sample contains a total of 4669 sources.

## 2.3. MMT Spectroscopy

To obtain redshifts for more X-ray AGN than were targeted in the DEEP2 survey (which began before the X-ray observations were taken, so X-ray sources were not given higher observing priority), we used the MMT/Hectospec fiber spectrograph for follow-up spectroscopy of optical counterparts to X-ray sources. We observed 5 Hectospec configurations in queue mode in May 2007, July 2007, and May 2008. Total integration times were 1.5-2 hours per configuration. The wave-

length coverage was  $\sim 4500 - 9000 \text{ \AA}$  at  $6 \text{ \AA}$  resolution. Observing conditions were fair, though not ideal; one night was affected by moonlight, and the seeing was often  $> 1''$ . Additional targets were observed as filler objects on configurations taken by other AEGIS team members (C. Willmer and P. Barnby, priv. comm.) during the same observing seasons, with similar spectrograph setups. In total, we targeted optical counterparts for 449 X-ray sources.

The data were reduced using the HSRED IDL reduction pipeline<sup>11</sup>. Redshifts were measured using a  $\chi^2$ -minimization between the observed spectrum and emission-line and absorption-line galaxy and AGN templates, and were confirmed by eye. We obtained high-confidence redshifts for 230 sources, or 51% of the targeted sample.

The spatial distribution of the X-ray AGN with redshifts between  $0.2 < z < 1.4$  is shown in Figure 1 (colored diamonds), along with the distribution of DEEP2 galaxies in the same redshift range (black squares). As discussed below in Section 3.2, galaxies and AGN in the upper quadrant are not used for the clustering measurements performed here; the green squares in Figure 1 show the X-ray AGN used to measure the cross-correlation function.

The  $R_{AB}$  magnitudes and  $B - R$  colors of the targeted sources and the subsample with successful redshift measurements are shown in Figure 2. Our success rate declines at  $R_{AB} > 22.5$ , as expected, as the signal-to-noise in the 2-hour spectra was not high enough to measure a robust redshift. A K-S test of the  $B - R$  color distribution for the targeted sources and the subsample with successful redshifts gives a 93% probability that they are drawn from the same parent population. The success rate is lowest at  $B - R \sim 1$ , but is comparable for red and blue galaxies.

Figure 3 shows the redshift distribution for all the X-ray sources with spectroscopic redshifts in the EGS (left), and split according to the instrument used to obtain spectroscopy (right). The left panel also shows the redshift distribution of DEEP2 galaxies in the EGS (dotted line), scaled down by a factor of 35. The redshift distribution for X-ray sources observed with Keck/DEIMOS (right panel) shows a peak at  $z \sim 0.7$  and a small tail of objects at  $z > 1.5$ , reflecting both the underlying redshift distribution of the  $R_{AB} < 24.1$  DEEP2 sources and the high resolution of the spectra, which results in a narrower spectral range of  $\sim 6500 - 9000 \text{ \AA}$ , limiting the redshifts where multiple features will be observed. The MMT/Hectospec redshift distribution is flatter and includes more objects at  $z > 1.5$ , due to the broader wavelength coverage of the spectra.

K-corrections, absolute  $M_B$  magnitudes and restframe  $(U - B)$  colors have been derived as described in Willmer et al. (2006). Absolute magnitudes given in this paper are in the AB system and are  $M_B - 5 \log(h)$  with  $h = 1$ , which for the remainder of the paper we denote as  $M_B$ . X-ray luminosities are derived using  $h = 0.7$ .

### 3. AGN PROPERTIES AND SAMPLES

#### 3.1. Optical Properties of X-ray AGN

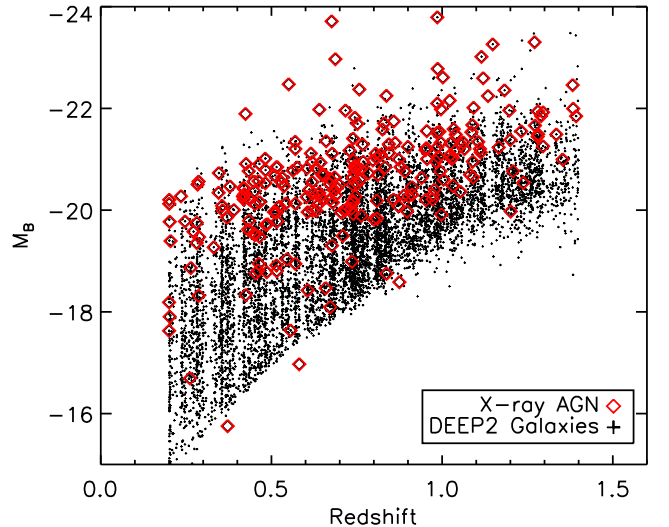


FIG. 4.— Absolute magnitude  $M_B$  as a function of redshift for DEEP2 galaxies in AEGIS (black crosses) and X-ray AGN (red diamonds). The AGN typically reside in optically bright galaxies, though they are occasionally found in fainter galaxies. AGN subsamples as a function of  $M_B$  are drawn to test the luminosity-dependence of AGN clustering.

Figure 4 shows the absolute magnitude,  $M_B$ , for the X-ray AGN host galaxies (red diamonds) and all DEEP2 galaxies (black crosses) as a function of redshift. The AGN tend to reside in optically bright galaxies, along the upper portion of the distribution, at all redshifts between  $z = 0.2 - 1.4$ . Figure 5 shows the color-magnitude diagram for the X-ray AGN (red diamonds) and DEEP2 galaxies (black crosses) in the redshift range  $z = 0.2 - 1.4$  (left) and  $z = 0.7 - 1.4$  (right). As originally shown in Nandra et al. (2007) and updated here with a larger sample (see also Barger et al. (2003)), X-ray AGN in the 200-ks depth *Chandra* AEGIS data predominantly have host galaxies that are either on the red sequence or the bright/red part of the blue cloud, implying that they reside in massive host galaxies (see also Silverman et al. 2008). X-ray AGN that are very bright and blue, with  $M_B < -21.3$  and  $(U - B) < 0.3$ , in the lower right corner of the figure, we define to be quasars, where the optical light is dominated by the AGN and not the host galaxy. ACS imaging of these sources in the EGS shows a bright blue point source with no host galaxy visible (Pierce et al. 2007, Georgakakis et al. in preparation). . 14% of the X-ray AGN in our sample at  $0.7 < z < 1.4$  are quasars, according to this definition. We note that contamination of the X-ray AGN sample by normal star-forming galaxies without AGN in this sample is expected to be less than 1% (Montero-Dorta et al. 2008).

In Figure 6 we compare the optical  $(U - B)$  color with the hardness ratio of the X-ray source, measured as  $HR \equiv (H - S)/(H + S)$ , where  $H = 2 - 7 \text{ keV}$  counts and  $S = 0.5 - 2 \text{ keV}$  counts. The hardness ratio estimates used here are determined through Bayesian methods and do not require detection in both the hard and soft bands; the actual source counts and background counts in both bands are used even if the object is not significantly detected. Therefore none of the X-ray AGN have  $HR = -1$  or  $HR = +1$ . The dashed line roughly marks

<sup>11</sup> See <http://www.astro.princeton.edu/~rcool/hsred>

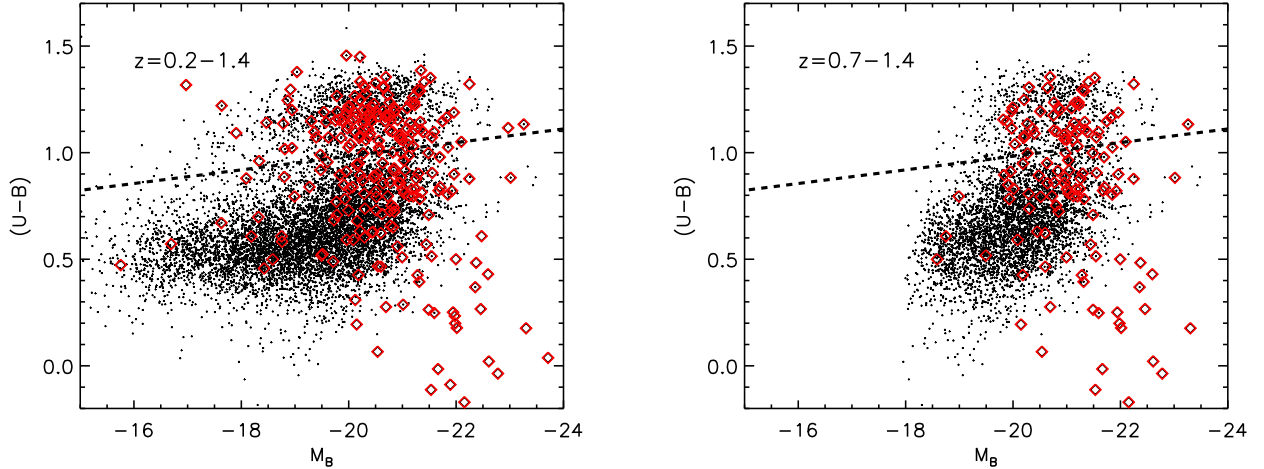


FIG. 5.— Restframe optical color-magnitude ( $(U-B)$  versus  $M_B$ ) diagram for DEEP2 galaxies (black crosses) and X-ray AGN (red diamonds) in AEGIS for the redshift ranges  $z = 0.2 - 1.4$  (left) and  $z = 0.7 - 1.4$  (right). The dashed line shows the definition of the minimum in the restframe  $(U-B)$  bimodality, used to define red and blue galaxies. X-ray AGN are predominantly found in red sequence galaxies, ‘green’ galaxies in the dip of the color bimodality, and the brightest/redest of the blue cloud galaxies. The optical light for a small percentage ( $\sim 14\%$ ) of the X-ray sources is dominated by the AGN itself and not the host galaxy; these sources are seen in the lower right corner and are optically very bright and blue.

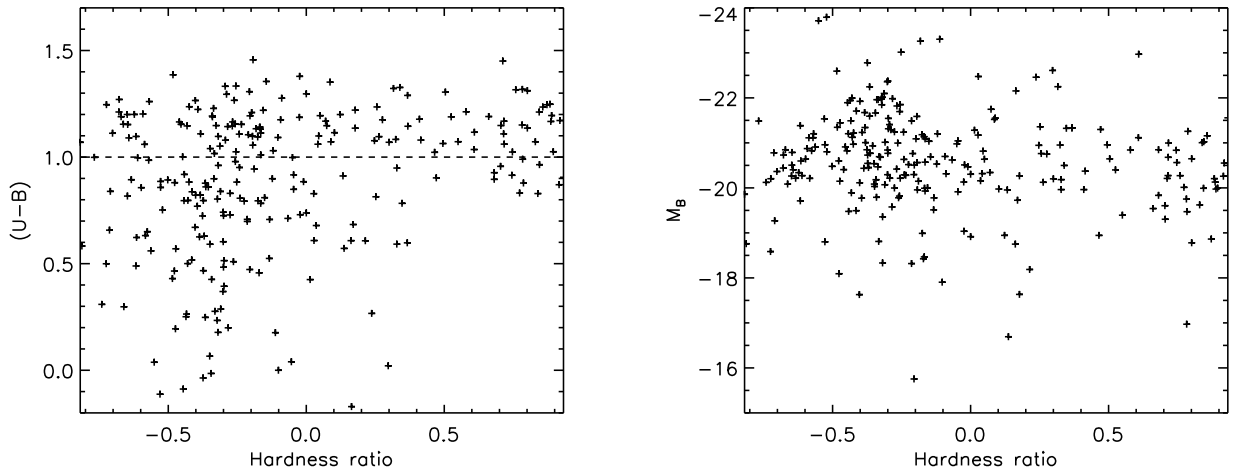


FIG. 6.— Left: Optical  $(U-B)$  color as a function of hardness ratio (see §3.1 for details) for all X-ray AGN in the redshift range  $z = 0.2 - 1.4$ . The dashed line roughly indicates the separation of red and blue galaxies, above and below the line respectively. The optically red and ‘green’ transition galaxies show a range of hardness ratios, while the blue galaxies are on average softer sources. Right: Optical absolute magnitude  $M_B$  as a function of hardness ratio for all X-ray AGN in the redshift range  $z = 0.2 - 1.4$ . A small but significant correlation is found between optical magnitude and hardness ratio.

the minimum of the color bimodality, with blue galaxies at  $(U-B) < 1.0$  and red galaxies at  $(U-B) > 1.0$ . We find a correlation between hardness ratio and optical obscuration in that the hardest X-ray sources are all optically red (e.g., Mainieri et al. 2002). This may either be the result of obscuration in the host galaxy itself, which reddens the galaxy as well as obscures the AGN, or it may be that obscured AGN only reside in galaxies with older stellar populations (Nandra et al. 2007; Rovilos & Georgantopoulos 2007). We find that the red and ‘green’ galaxies have a wide range of hardness ratios, while the blue galaxies are softer sources. A small but significant correlation is found between absolute magnitude  $M_B$  and hardness ratio, which have a Spearman’s rank correlation coefficient of  $\rho = 0.14$  at 97% significance. This correlation persists after excluding the

brightest sources with  $M_B < -22$ , indicating that it is not likely to be dominated by an increased contribution from unobscured AGN.

### 3.2. AGN samples

From the full AGN and galaxy datasets we define several samples used to measure the AGN-galaxy cross-correlation function. We limit most samples to the redshift range  $0.7 < z < 1.4$  so as to match the redshift range of the other DEEP2 fields where we have performed extensive clustering analyses of galaxies as a function of color and luminosity (Coil et al. 2006a, 2008), as well as the measurement of the quasar-galaxy cross-correlation function (Coil et al. 2007), with which we compare our results here. We do not include data from the upper quadrant of the EGS field (pointing 14 in the DEEP2

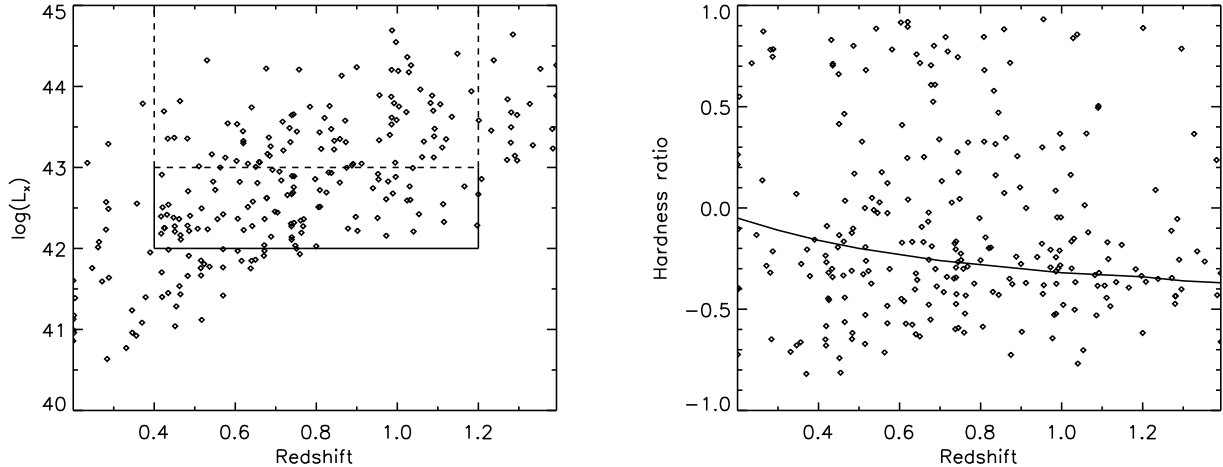


FIG. 7.— Left: X-ray luminosity as a function of redshift for all X-ray AGN in the redshift range  $z = 0.2 - 1.4$ . The ‘AGN high  $L_X$ ’ and ‘AGN low  $L_X$ ’ samples are defined by the dashed and solid lines, respectively. Right: Hardness ratio of the X-ray AGN as a function of redshift. The ‘AGN hard’ and ‘AGN soft’ samples are defined as being above or below the solid line, corresponding to  $N_H = 10^{22} \text{ cm}^{-2}$  for  $\Gamma = 1.9$ .

TABLE 1  
AGN AND GALAXY SAMPLES

Sample	No. of objects	$z$ range	median $z$	median $M_B$	selection <sup>a</sup>
AGN main	113	0.7-1.4	0.90	-20.98	does not include quasars
AGN host bright	54	0.7-1.4	1.00	-21.33	$M_B < -21$
AGN host faint	59	0.7-1.4	0.84	-20.45	$M_B > -21$
AGN host red	50	0.7-1.4	0.90	-20.96	red $(U - B)$ host galaxy
AGN host blue	63	0.7-1.4	0.91	-20.98	blue $(U - B)$ host galaxy
AGN low $L_X$	91	0.4-1.2	0.74	-20.40	$42 < \log L_X < 43 \text{ erg s}^{-1}$
AGN high $L_X$	83	0.4-1.2	0.84	-21.01	$\log L_X > 43 \text{ erg s}^{-1}$
AGN hard	140	0.2-1.4	0.75	-20.62	$N_H > 10^{22} \text{ cm}^{-2}$
AGN soft	111	0.2-1.4	0.67	-20.60	$N_H < 10^{22} \text{ cm}^{-2}$
All galaxies	4669	0.7-1.4	0.92	-20.16	
Red galaxies	757	0.7-1.4	0.85	-20.66	red $(U - B)$
Blue galaxies	3913	0.7-1.4	0.94	-20.06	blue $(U - B)$
Matched galaxies	504	0.7-1.4	0.98	-20.97	
Red matched galaxies	226	0.7-1.4	0.92	-20.92	
Blue matched galaxies	278	0.7-1.4	1.03	-20.99	

<sup>a</sup> See Section 3 for details on each AGN sample and Section 5 for details on each galaxy sample.

naming convention), where the DEEP2 target selection function is slightly different from the rest of the survey, due to shallower  $BRI$  photometric imaging (Coil et al. 2004a) used in the target selection. The total area covered by the data used here is  $\sim 0.4 \text{ deg}^2$ .

Details of each AGN sample are given in Table 1. The ‘AGN main’ sample includes all non-quasar X-ray AGN over the redshift range  $z = 0.7 - 1.4$ , a total of 113 sources; as seen in the left panel of Figure 7 these AGN have  $\log L_X > 42 \text{ erg s}^{-1}$ , where  $L_X$  is the restframe 2-10 keV luminosity calculated from the observed 2-10 keV flux, assuming a photon index  $\Gamma = 1.9$ .

The main AGN sample has a mean  $\log L_X = 42.4 \text{ erg s}^{-1}$  and a median  $\log L_X = 42.8 \text{ erg s}^{-1}$ . The ‘AGN host bright’ and ‘AGN host faint’ samples are defined by their optical  $M_B$  magnitude; the samples are split at the median  $M_B$  magnitude of the AGN main sample. The ‘AGN host red’ and ‘AGN host blue’ samples are defined by the optical color of the host galaxy. Following Willmer et al. (2006), we define red and blue galax-

ies using the observed color bimodality in DEEP2 with the following tilted cut in color-magnitude space (in AB magnitudes):

$$(U - B) = -0.032(M_B + 21.62) + 1.035, \quad (1)$$

as shown in Figure 5. We do not allow this color cut to evolve with redshift within the redshift range used here.

For the AGN samples defined by optical color or magnitude we exclude the quasars in the lower right portion of Figure 5, as the optical color and magnitude of these objects is not reflective of the host galaxy but is from the AGN itself. We define quasars here as sources with  $M_B < -21.3$  and  $(U - B) < 0.3$ ; there are 19 quasars in our sample with  $0.7 < z < 1.4$  (12 of which are shown in the right panel of Figure 5, the rest are outside the plot range), out of 132 X-ray sources. None of our results change if these sources are included. For the ‘AGN host bright/faint’ and ‘AGN host red/blue’ samples, the optical magnitude and color are properties of the host galaxy, not the AGN itself. The sample of spectroscopically-



identified broad-line AGN is too small to use for robustly measure clustering properties; a larger sample is needed.

We also divide the full AGN sample by X-ray luminosity, using the median value of  $\log L_X = 43 \text{ erg s}^{-1}$ , such that the ‘AGN low  $L_X$ ’ sample is defined as having  $42 < \log L_X < 43 \text{ erg s}^{-1}$  (which results in a roughly volume-limited sample), while the ‘AGN high  $L_X$ ’ sample has  $\log L_X > 43 \text{ erg s}^{-1}$ , as shown in the left panel of Figure 7. Since here we are concerned with comparing the  $L_X$  samples to each other and not to galaxies in the same redshift range, we are free to use a different redshift range from that used in the DEEP2 galaxy clustering studies. For the  $L_X$ -selected samples we use a lower redshift limit of  $z = 0.4$ , which increases the sample size but is not so low as to cause the two samples to have significantly different mean redshifts (see Table 1). To keep the ‘AGN low  $L_X$ ’ sample roughly volume-limited we use an upper redshift limit of  $z = 1.2$  (see Figure 7), which ensures that any difference seen in their clustering properties should be dominated by differences in luminosity and not redshift. The ‘AGN hard’ and ‘AGN soft’ samples are defined by the X-ray color, or hardness ratio, as shown in the right panel of Figure 7. The solid line corresponds to  $N_H = 10^{22} \text{ cm}^{-2}$  for  $\Gamma = 1.9$  and defines the ‘AGN hard’ and ‘AGN soft’ samples. For these samples we use the full redshift range of  $z = 0.2 - 1.4$ .

Several galaxy samples are used in this paper; details for each are given in Table 1. All cross-correlation functions presented here use the full DEEP2 galaxy sample with  $0.7 < z < 1.4$  (‘All galaxies’ in Table 1) to cross-correlate with either an AGN or a galaxy sample. This full galaxy sample is separated into red and blue galaxy samples based on restframe  $(U - B)$  color, with the color cut given above. Matched galaxy samples are discussed in §5.3; these samples have the same  $M_B$  and  $(U - B)$  distributions as various comparison AGN samples.

#### 4. MEASURING THE CROSS-CORRELATION FUNCTION

To measure the clustering of the X-ray AGN sample, we use the cross-correlation of AGN with galaxies in the same volume, and the auto-correlation function of the galaxies themselves, to infer the auto-correlation function of the AGN sample.

The two-point auto-correlation function  $\xi(r)$  is defined as a measure of the excess probability above that for an unclustered distribution of finding an object in a volume element  $dV$  at a separation  $r$  from another randomly chosen object,

$$dP = n[1 + \xi(r)]dV, \quad (2)$$

where  $n$  is the mean number density of the object in question (Peebles 1980). The cross-correlation function is the excess probability above Poisson of finding an object from a given sample at a separation  $r$  from a random object in another sample. Here we measure the cross-correlation between AGN and galaxies:

$$dP(G|A) = n_G[1 + \xi_{AG}(r)]dV, \quad (3)$$

which is the probability of finding a galaxy ( $G$ ) in a volume element  $dV$  at a separation  $r$  from an AGN ( $A$ ), where  $n_G$  is the number density of galaxies.

To estimate the cross-correlation function between our AGN and galaxy samples, we measure the observed number of galaxies around each AGN as a function of distance, divided by the expected number of galaxies for a

random distribution. We use the estimator

$$\xi = \frac{AG}{AR} - 1, \quad (4)$$

where  $AG$  are AGN-galaxy pairs and  $AR$  are AGN-random pairs at a given separation, where the pair counts have been normalized by  $n_G$  and  $n_R$ , respectively, the mean number densities in the full galaxy and random catalogs. This estimator is preferred here as it does not require knowledge of the AGN selection function, only the galaxy selection function, which is well-quantified. To calculate  $\xi(r)$  we create a random catalog with the same redshift distribution as the DEEP2 galaxies used for the cross-correlation measurement and the same sky coverage as the DEEP2 galaxies in the EGS, applying the two-dimensional variation in the DEEP2 target selection and redshift success rate over the plane of the sky. We also mask the regions of the random catalog where the photometric data are affected by saturated stars or CCD defects. Details on the random catalog construction are given in §3.1 of Coil et al. (2004b).

We wish to measure the real-space correlation function,  $\xi(r)$ . However, peculiar velocities distort the positions of objects in redshift space along the line of sight. To capture this effect, we measure  $\xi$  as a function of two coordinates, perpendicular to  $(r_p)$  and along  $(\pi)$  the line of sight. In applying the above estimator to galaxies, pair counts are computed over a two-dimensional grid of separations to estimate  $\xi(r_p, \pi)$ . To recover  $\xi(r)$ ,  $\xi(r_p, \pi)$  is integrated along the  $\pi$  direction and projected onto the  $r_p$  axis. As redshift-space distortions affect only the line-of-sight component of  $\xi(r_p, \pi)$ , integrating over the  $\pi$  direction leads to a statistic  $w_p(r_p)$ , which is independent of redshift-space distortions. Following Davis & Peebles (1983),

$$w_p(r_p) = 2 \int_0^\infty d\pi \xi(r_p, \pi) = 2 \int_0^\infty dy \xi[(r_p^2 + y^2)^{1/2}], \quad (5)$$

where  $y$  is the real-space separation along the line of sight. Here, as in other DEEP2 clustering studies, we integrate to a maximum separation in the  $\pi$  direction of  $20 h^{-1} \text{ Mpc}$ , as the signal to noise degrades quickly for larger separations where  $\xi$  becomes small. Systematic effects due to the use of slitmasks are small (see §3.4 of Coil et al. (2008) for details). We do not correct for these effects here, as we are primarily concerned with the *relative* clustering of AGN samples compared to each other and to the clustering of galaxy samples, and to first order these effects will cancel.

Error bars on  $w_p(r_p)$  are estimated from jackknife sampling of the data, where the EGS is divided into eight regions of equal area and  $w_p(r_p)$  is calculated for eight jackknife samples, removing one area at a time. To check the validity of these jackknife error bars, we compare the  $w_p(r_p)$  errors for the ‘main AGN sample’ with errors that include both Poisson and cosmic variance errors estimated using DEEP2 mock catalogs derived from the Millenium Run simulation (see Kitzbichler & White 2007, for further details). Using a total of 24 independent mock catalogs with the same geometry and selection function as the DEEP2 data in the EGS, we select 113 random red galaxies with  $0.7 < z < 1.4$  to be X-ray AGN proxies, since red DEEP2 galaxies have a similar clustering amplitude as the X-ray AGN, as shown below



TABLE 2  
RELATIVE BIAS RESULTS

Samples	Relative bias	
	$0.1 < r_p < 8 \ h^{-1} \text{ Mpc}$	$1 < r_p < 8 \ h^{-1} \text{ Mpc}$
AGN host bright/faint	$1.52 \pm 0.32$	$1.20 \pm 0.31$
AGN host red/blue	$1.91 \pm 0.38$	$1.79 \pm 0.27$
AGN high $L_x$ /low $L_x$	$1.05 \pm 0.18$	$0.95 \pm 0.20$
AGN hard/soft	$1.22 \pm 0.12$	$1.27 \pm 0.17$
AGN/Red galaxies	$0.97 \pm 0.07$	$0.94 \pm 0.08$
AGN/Blue galaxies	$1.61 \pm 0.11$	$1.48 \pm 0.12$
AGN/Matched galaxies	$1.28 \pm 0.10$	$1.15 \pm 0.09$
AGN host red/Red galaxies	$1.20 \pm 0.09$	$1.13 \pm 0.09$
AGN host red/Red matched galaxies	$1.33 \pm 0.15$	$1.19 \pm 0.12$
AGN host blue/Blue galaxies	$1.27 \pm 0.15$	$1.22 \pm 0.13$
AGN host blue/Blue matched galaxies	$1.24 \pm 0.16$	$1.09 \pm 0.16$

in Section 5.3. We calculate the cross-correlation of these AGN proxy galaxies with all mock DEEP2-like galaxies in each mock catalog, and then calculate the variance across the 24 catalogs. The error on  $w_p(r_p)$  in the mock catalogs is less than the error estimated from jackknife sampling of the data itself: on scales  $r_p=1-8 \ h^{-1} \text{ Mpc}$  in the mock catalogs the fractional error on  $w_p(r_p)$  is 8%, while in the data it is 10%. To be conservative we therefore use the error estimated from the jackknife samples of the data. As previously noted (Coil et al. 2007), the Millenium Run mock catalogs appear to exhibit smaller variance than the real Universe.

If  $\xi(r)$  is modeled as a power law,  $\xi(r) = (r/r_0)^{-\gamma}$ , then  $r_0$  and  $\gamma$  can be readily extracted from the projected correlation function,  $w_p(r_p)$ , using an analytic solution to Equation 5:

$$w_p(r_p) = r_p \left( \frac{r_0}{r_p} \right)^\gamma \frac{\Gamma(\frac{1}{2})\Gamma(\frac{\gamma-1}{2})}{\Gamma(\frac{\gamma}{2})}, \quad (6)$$

where  $\Gamma$  is the usual gamma function. A power-law fit to  $w_p(r_p)$  will then recover  $r_0$  and  $\gamma$  for the real-space correlation function,  $\xi(r)$ . In practice, however, we can not measure  $\xi(r_p, \pi)$  accurately to infinite separations as assumed in Equation 5, and here we integrate  $w_p(r_p)$  to  $\pi_{\max} = 20 \ h^{-1} \text{ Mpc}$ . To recover the correlation length and slope we then estimate  $w_p(r_p)$  integrated to  $\pi_{\max} = 20 \ h^{-1} \text{ Mpc}$  for a grid of  $r_0$  and  $\gamma$  values and minimize the difference between the data and model. Full details are given in §4.2 of Coil et al. (2008). We do not use a full covariance matrix in the fits. Errors on  $r_0$  and  $\gamma$  are propagated from the jackknife errors on  $w_p(r_p)$ ; if instead we measure  $r_0$  and  $\gamma$  in the separate jackknife samples and use the variance among the various fits, which does take into account the covariance between the  $r_p$  bins, the resulting errors are somewhat smaller. To be conservative we use the larger errors derived from the  $w_p(r_p)$  errors.

## 5. RESULTS

### 5.1. Clustering of Main AGN Sample

The projected cross-correlation of the ‘AGN main’ sample with all DEEP2 galaxies in the same redshift range,  $w_p(r_p)$ , is shown with a dashed red line in Figure 8. As discussed above, the  $w_p(r_p)$  error bars are derived from jackknife samples of the data and are slightly larger than errors inferred from cosmological simulations.

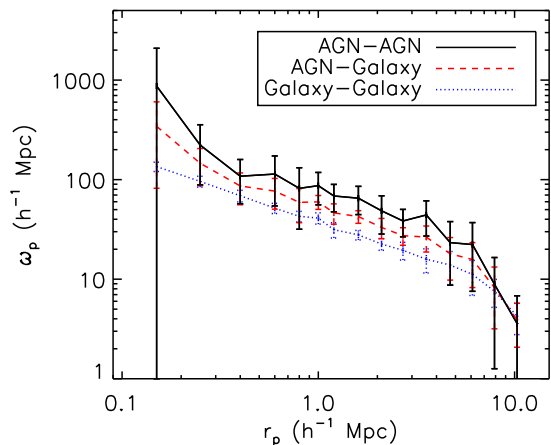


FIG. 8.— The projected AGN-galaxy cross-correlation function  $w_p(r_p)$  as a function of scale for the non-quasar X-ray AGN main sample (red dashed line) and the full DEEP2 galaxy population in the EGS with  $0.7 < z < 1.4$ . The galaxy auto-correlation function in the same volume is shown (blue dotted line), as well as the inferred X-ray AGN auto-correlation function (black solid line). Errors are computed from jackknife samples of the data and are comparable to errors found from mock catalogs (see text for details).

The projected galaxy auto-correlation function is also shown (blue dashed line) for the full galaxy sample with  $0.7 < z < 1.4$ . Assuming a linear bias,

$$w_p(AG) = [w_p(AA) \times w_p(GG)]^{1/2}, \quad (7)$$

where  $w_p(AG)$  is the AGN-galaxy cross-correlation function, and  $w_p(AA)$  and  $w_p(GG)$  are the AGN and galaxy auto-correlation functions. From measurements of  $w_p(AG)$  and  $w_p(GG)$ , as shown in Figure 8, the X-ray AGN auto-correlation function  $w_p(AA)$  can then be inferred; this is shown in Figure 8 as a solid black line, where the errors are derived from jackknife resampling of  $w_p(AG)^2/w_p(GG)$ .

Fitting  $w_p(AA)$  as a power law, we find  $r_0 = 5.95 \pm 0.90 \ h^{-1} \text{ Mpc}$  and  $\gamma = 1.66 \pm 0.22$ . To compute the bias of the X-ray AGN auto-correlation function compared to that expected for dark matter, we estimate  $w_p(r_p)$  for dark matter particles at the mean redshift of the main AGN sample, using the publicly-available code of Smith et al. (2003), where we integrate the dark matter  $\xi(r_p, \pi)$  to  $\pi_{\max} = 20 \ h^{-1} \text{ Mpc}$ . We estimate the linear galaxy bias from the ratio of the quantities  $b^2 =$

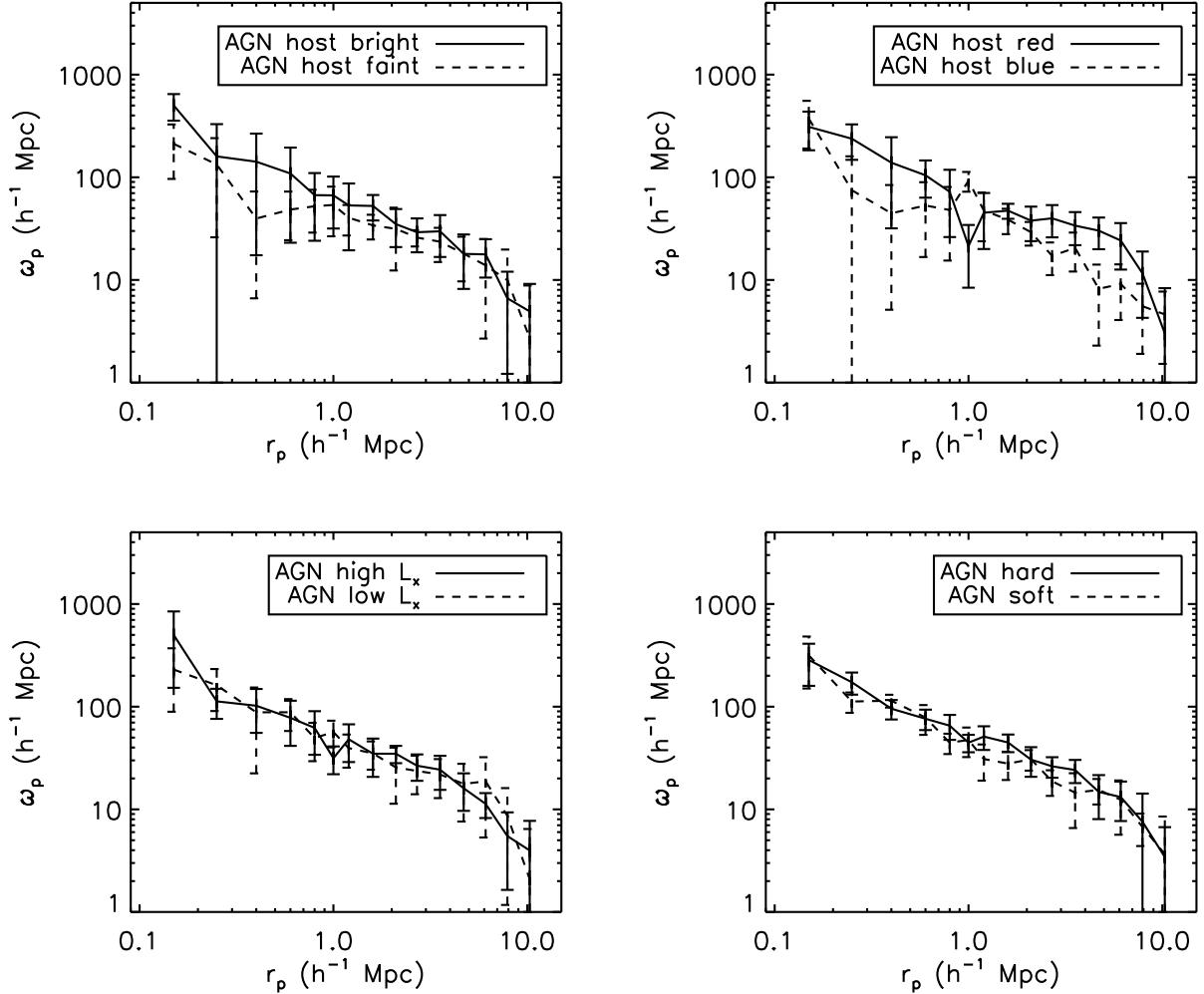


FIG. 9.— The projected AGN-galaxy cross-correlation functions for AGN samples split according to optical  $M_B$  magnitude (upper left), optical ( $U - B$ ) color (upper right), X-ray luminosity (lower left), and X-ray color or hardness ratio (lower right). Details of each sample are given in Table 1. No significant difference in clustering is detected for the samples selected on optical luminosity, X-ray luminosity or X-ray color. There is a correlation with optical color: the X-ray AGN with red host galaxies are significantly more clustered than those in blue host galaxies.

$[w_p]_{\text{gal}}/[w_p]_{\text{dark matter}}$ , and average over scales  $1 < r_p < 8$   $h^{-1}$  Mpc, to find a mean bias of  $b = 1.85 \pm 0.28$ .

From the bias of the main AGN sample we can infer the minimum dark matter mass for halos that host these AGN. As shown in the Appendix of Zheng, Coil, & Zehavi (2007), the dark matter mass inferred assuming that all objects, whether galaxies or AGN, are ‘central’ objects in their dark matter halos (ie., assuming one galaxy or AGN per halo) can lead to an overestimate of the minimum halo mass. Here we assume that the AGN population has the same satellite fraction, or number of additional galaxies per halo, as found in the DEEP2 galaxy population using HOD modeling of the correlation function, where the satellite fraction is  $\sim 15\%$  (Zheng, Coil, & Zehavi 2007). Using this correction for the satellite fraction changes the relative weights given to halos of a different mass when computing the large-scale bias for different halo masses, and the minimum mass inferred is slightly lower than assuming one AGN per halo. Here we find that at  $z = 0.94$  the minimum dark matter halo mass of the non-quasar

X-ray AGN is  $M_{\text{min}} = 5 (+5/-3) \times 10^{12} h^{-1} M_{\odot}$ , similar to red galaxies at the same redshift (Coil et al. 2008).

## 5.2. Clustering of Other AGN Samples

To investigate the dependencies of AGN clustering properties, we divide the main AGN sample into samples based on optical luminosity, optical color, X-ray luminosity and hardness ratio. Details of the selection for each sample are given in Section 3 and in Table 1. Figure 9 shows the projected cross-correlation with the DEEP2 galaxies,  $w_p(r_p)$ , for each of these samples. To quantify differences in clustering amplitude, we calculate the relative bias between these samples. The relative bias is defined here as the ratio of  $w_p(r_p)$  for two samples. Note that this is the usual meaning of relative bias ( $b_{\text{rel}}^2 = \xi_1/\xi_2$ ), as here we are using cross-correlation functions with the identical galaxy tracer samples and not auto-correlation functions. The error bars on the relative bias measurement are not estimated from the errors on  $w_p(r_p)$  directly, as that would not include covariance between the bins and would include cosmic variance errors, which cancel to first order when comparing

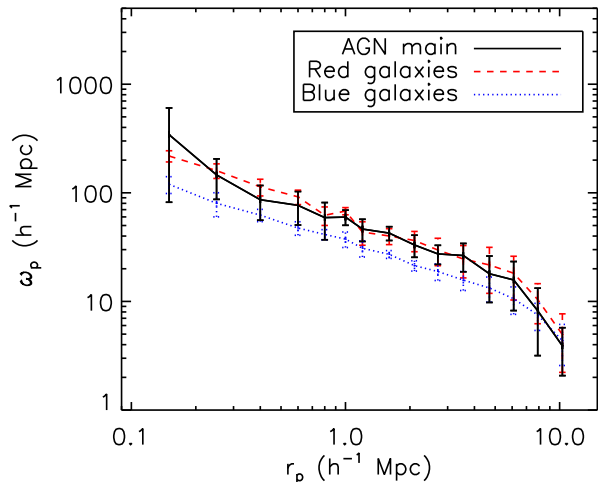


FIG. 10.— The projected AGN-galaxy cross-correlation function  $w_p(r_p)$  as a function of scale for the AGN main sample (black solid line) and the full DEEP2 galaxy sample with  $0.7 < z < 1.4$ . The cross-correlations of red and blue DEEP2 galaxies with the full galaxy sample in the same volume are also shown with dashed red and dotted blue lines, respectively. The X-ray AGN are seen to have very similar clustering properties to red galaxies and are more clustered than blue galaxies at  $z \sim 1$ .

the clustering of two populations in the same volume. The relative bias errors are therefore estimated from the variance of the relative bias measured across the jackknife samples.

As the relative bias can be scale-dependent, we calculate the unweighted mean relative bias over two scales,  $r_p = 0.1 - 8 h^{-1}$  Mpc (‘all scales’) and  $r_p = 1 - 8 h^{-1}$  Mpc (‘large scales’), and also measure the variance of the relative bias on the same scales. Relative bias results for various samples are given in Table 2. We find no significant difference in the clustering of AGN when selected by optical luminosity, X-ray luminosity, or hardness ratio, within the ranges sampled here. We find that the AGN in red host galaxies are significantly more clustered than those in blue host galaxies, at the  $2.9\sigma$  level on large scales, with a relative bias of  $b_{rel} = 1.79 \pm 0.27$ , and at the  $2.4\sigma$  level on all scales, with a relative bias of  $b_{rel} = 1.91 \pm 0.38$ . This relative bias is consistent with the relative bias found between red and blue DEEP2 galaxies of  $b_{rel} = 1.44 \pm 0.07$  measured in Coil et al. (2008).

We do not find a significant difference in the clustering of hard X-ray sources compared to soft X-ray sources. This lack of a detectable correlation between hardness ratio and clustering amplitude may be surprising, given that we observe correlations both between host ( $U - B$ ) color and hardness ratio (in that the hardest sources are in optically red host galaxies, see Figure 6) and between host ( $U - B$ ) color and clustering amplitude, both using smaller samples than for the hardness ratio-clustering comparison. One reason for the lack of a significant correlation between hardness ratio and clustering amplitude may be the large range of hardness ratios among the red AGN host galaxies (see Figure 6), so that while the hard sample is dominated by red galaxies, the soft sample has both red and blue galaxies, mitigating the effect of the hardness-color and color-clustering correlations. Our results clearly show that AGN host color is more correlated

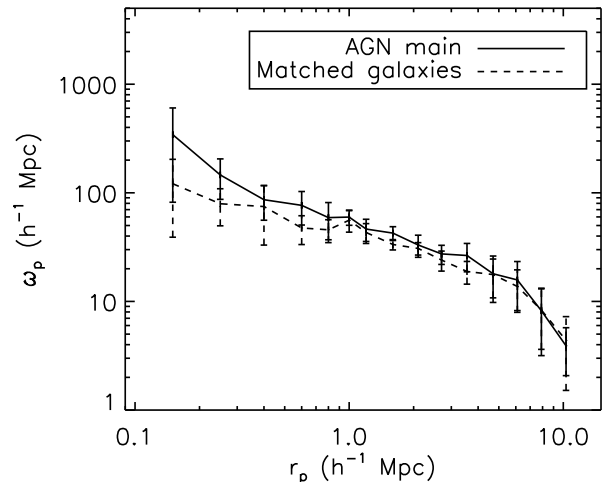


FIG. 11.— The projected AGN-galaxy cross-correlation function  $w_p(r_p)$  for the AGN main sample compared to the cross-correlation function of a sample of galaxies with the same optical color and magnitude distribution, regardless of whether they host AGN. Those galaxies with X-ray AGN are found to cluster more than the full galaxy population with the same color and luminosity distribution, which implies that they reside in more massive dark matter halos.

with dark matter halo mass than hardness ratio is: i.e., star formation histories are more closely related to local environment than AGN X-ray hardness is.

### 5.3. Clustering of AGN Compared to Galaxies

In Figure 10 we compare the main AGN sample with the clustering of red and blue DEEP2 galaxies in the same volume. Here we have computed the cross-correlation of red or blue DEEP2 galaxies with all DEEP2 galaxies, similar to the AGN-galaxy cross-correlation measurement. We use all red and blue DEEP2 galaxies, without an absolute magnitude limit, to ensure that the redshift distribution of the red and blue galaxies is similar to that of the X-ray AGN. The median absolute magnitudes of the galaxy samples are  $M_B = -20.1$  for the blue galaxies and  $M_B = -20.7$  for the red galaxies. If we do impose a limit of  $M_B < -20$  for the blue galaxies it does not change the result; the relative bias is within  $1\sigma$  of the value using all blue DEEP2 galaxies.

The X-ray AGN are seen to have a similar clustering amplitude as red DEEP2 galaxies and are more clustered than blue DEEP2 galaxies. The relative bias of the main AGN sample to red galaxies is  $b_{rel} = 0.94 \pm 0.08$  on large scales and  $b_{rel} = 0.97 \pm 0.07$  on all scales, while the relative bias to blue galaxies is  $b_{rel} = 1.48 \pm 0.12$  on large scales and  $b_{rel} = 1.61 \pm 0.11$  on all scales. The X-ray AGN are significantly more clustered than blue galaxies at  $z \sim 1$ .

The slope of the X-ray AGN correlation function is more similar to that of blue DEEP2 galaxies than red DEEP2 galaxies (Coil et al. 2008), but within  $2\sigma$  it is consistent with either. As seen in Figure 8, the X-ray AGN correlation function may have a steeper slope on small scales,  $r_p < 0.5 h^{-1}$  Mpc, compared to all galaxies, but the error bars on the X-ray AGN  $w_p(r_p)$  are too large to detect a significant difference.

While the main AGN sample has the same clustering

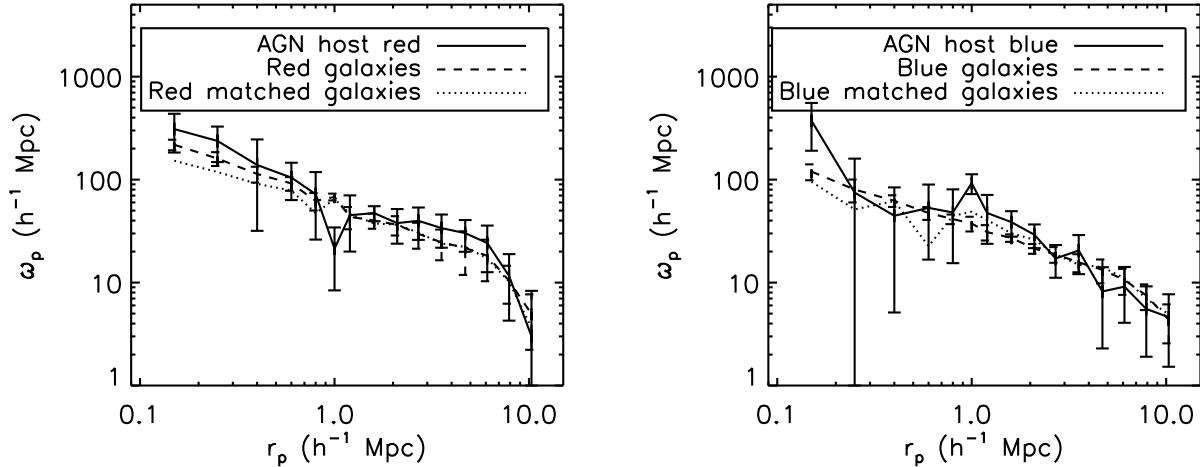


FIG. 12.— The clustering of AGN host galaxies compared to all galaxies of a given color. Left: The projected AGN-galaxy cross-correlation function  $w_p(r_p)$  as a function of scale for AGN in red host galaxies (solid line) compared to all red galaxies (dashed line) and red galaxies with the same color and magnitude distribution (dotted line) at  $0.7 < z < 1.4$ . Right: The projected AGN-galaxy cross-correlation for AGN in blue host galaxies (solid line) compared to all blue galaxies (dashed line) and blue galaxies with the same color and magnitude distribution (dotted line) at  $0.7 < z < 1.4$ . Galaxies which host AGN are found to be somewhat more clustered than galaxies of the same color and magnitude, especially on scales  $r_p < 1 h^{-1}$  Mpc.

amplitude as red galaxies at  $z \sim 1$ , only half (42%) of X-ray AGN are in red host galaxies. This implies that AGN in red galaxies may be more clustered than red galaxies as a whole and/or that AGN in blue galaxies may be more clustered than blue galaxies as a whole. It also implies that galaxies of a given color and luminosity distribution that host X-ray AGN may be more clustered than those without AGN.

We can test this by comparing the clustering of the main AGN sample with that of DEEP2 galaxies with the same color and magnitude distribution as the AGN host sample; the results are shown in Figure 11. To create the ‘matched galaxy sample’ to compare with the main AGN sample, we first measure the joint color-magnitude distribution of the main AGN sample in  $(U - B)$  and  $M_B$  space, in bins of 0.1 in  $(U - B)$  color and 0.3 in  $M_B$  magnitude. We then normalize this distribution to have a maximum value of 1, making it effectively a relative weight map in color-magnitude space. We then select all DEEP2 galaxies in the same volume as the main AGN sample, and for each bin in color-magnitude space we randomly sample the galaxy population (without replacement) such that the fraction of the final sample in that bin is equal to the weight in the main AGN sample. We have tested that creating a matched sample with replacement from the parent population does not change the results within the  $1\sigma$  error bars. The matched sample therefore has a nearly identical joint distribution in color-magnitude space as the main AGN sample. The resulting cross-correlation of this ‘matched galaxy sample’ with all DEEP2 galaxies in the same volume is shown as the dashed line in Figure 11. The AGN are seen to cluster more than the matched galaxy sample at the  $2.8\sigma$  level when measured on scales  $0.1 < r_p < 8 h^{-1}$  Mpc, with a relative bias of  $b_{rel} = 1.28 \pm 0.10$ , and  $b_{rel} = 1.15 \pm 0.09$  on scales  $1 < r_p < 8 h^{-1}$  Mpc. Galaxies of a given optical color and luminosity which host an AGN are therefore more clustered than their quiescent counterparts.

The higher clustering amplitude found for AGN in red

galaxies compared to AGN in blue galaxies could possibly be more fundamentally tied to the stellar mass of the host galaxy rather than its optical color; determining which is more fundamental is beyond the scope of this paper. However, the enhanced clustering amplitude found here for AGN compared to galaxies with the same color and magnitude distribution can *not* be due to a difference in stellar mass between the populations; ie, the clustering difference can not be due to AGN being hosted in more massive galaxies. The stellar mass of DEEP2 galaxies is tightly correlated with the  $(U - B)$  color and  $M_B$  magnitude (see Figure 10 in Weiner et al. (2009)), such that the matched galaxy samples have similar stellar mass distributions as the AGN.

We further compare the clustering of the AGN in red and blue galaxies to the full red and blue galaxy samples and also to red and blue galaxy samples with the same color and magnitude distribution (‘matched’ red and blue samples) in Figure 12. The relative biases for these samples are given in Table 2. There are only minor differences between the biases for matched galaxy samples and the full red or blue galaxy samples. We find that AGN in red host galaxies are more clustered than both all red galaxies and matched red galaxies at the  $2.2\sigma$  level when combining measurements from all scales, and on large scales they are not significantly more clustered. The relative bias is similar to that from comparing all AGN to all matched galaxies, but the error bars are larger on the red subsamples and the significance is lower. Comparing the clustering of AGN in blue host galaxies with matched blue galaxies, we do not find a significant difference in their clustering properties, though again the relative bias is consistent with that for all AGN and all matched galaxies; the error bars for the blue subsamples are simply too large to say if there is a significant difference in clustering or not. The difference that we find between the clustering of the main AGN sample and all matched galaxies may therefore either be dominated by a difference in the clustering of red galaxies with and

without AGN or be due to both red and blue galaxies.

## 6. DISCUSSION

We find here that non-quasar X-ray AGN, taken as an ensemble, have a similar clustering amplitude as red, quiescent galaxies at  $z \sim 1$ . Our results confirm and extend the findings of Georgakakis et al. (2007), who found that a smaller sample of X-ray AGN in AEGIS had environments similar to those of red galaxies. Not all of the X-ray AGN are hosted by red galaxies, however; roughly half are in galaxies whose optical color is blue. Visual inspection of ACS imaging in the AEGIS field (Davis et al. 2007) confirms that the optical light in the X-ray AGN host galaxies is not dominated by the AGN itself, but by galaxy light (see also Figure 2 of Nandra et al. (2007)); the exception to this is the 14% of X-ray AGN that we define as quasars, where the optical light is from the AGN itself and is very bright and blue. We find that the X-ray AGN in red host galaxies are more clustered than those in blue host galaxies, and that when compared to galaxy samples with the same color and luminosity distribution (and hence, stellar mass), those galaxies with X-ray AGN are somewhat more clustered.

### 6.1. Comparison to Other X-ray Clustering Studies

Figure 13 compares the correlation scale length found for various AGN and galaxy samples at  $z \sim 0 - 1$ . We find here that X-ray AGN at a median  $z = 0.94$  with a median luminosity of  $\log L_x = 42.8 \text{ erg s}^{-1}$  have a correlation length of  $r_0 = 5.95 \pm 0.90 \text{ } h^{-1} \text{ Mpc}$  and  $\gamma = 1.66 \pm 0.22$ . This clustering scale length is similar to that found by Gilli et al. (2005), Yang et al. (2006), and Gilli et al. (2009) for the CDFN and CLASXS and COSMOS fields and differs from that found by Gilli et al. (2005) for the CDFS field; these are the only other studies at  $z \sim 1$  that use spectroscopic redshifts to measure the correlation function of X-ray AGN. At lower redshift, Mullis et al. (2004) find a consistent correlation length of  $r_0 = 7.4 \pm 1.9 \text{ } h^{-1} \text{ Mpc}$  for a fixed slope of  $\gamma = 1.8$ ; however, a comparison with this result is complicated due to the brighter nature of the sources (median  $\log L_x = 44 \text{ erg s}^{-1}$ ) and larger measurement scales ( $r_p = 5 - 100 \text{ } h^{-1} \text{ Mpc}$ ). The correlation slope that we find,  $\gamma = 1.66 \pm 0.22$ , is consistent with that found by Gilli et al. (2005), Yang et al. (2006), and Gilli et al. (2009), which are measured on similar scales to those used here.

Our results are in modest disagreement with those of Montero-Dorta et al. (2008), who study the environment-dependence within the red sequence of various AGN classes in DEEP2, including optically-selected LINERs, Seyferts, and X-ray AGN, and find that while LINERs in red host galaxies are more likely to be in over-dense regions, Seyferts and X-ray AGN do not have any environment-dependence relative to red galaxies with the same magnitude distribution as the AGN population. In contrast, we find here that X-ray AGN in red galaxies are biased relative to a galaxy population matched in color and magnitude at the  $2\sigma$  level. However, only 36 X-ray sources were used in that study, which may account for the discrepancy with our findings here.

Measuring the cross-correlation function of X-ray sources with galaxies, as is done here, has several benefits. One is that the spatial selection function and red-

shift completeness for one of the samples, either the AGN or the galaxies, does not need to be known, as long as the selection function of the other sample is well characterized. By using the cross-correlation of the X-ray sources with galaxies, we do not need to include the selection function for the X-ray AGN. When measuring the auto-correlation function of X-ray sources, one must carefully model both the spatial selection function, including the varying X-ray sensitivity across the field, and the spectroscopic completeness, so as not to bias the results. All auto-correlation function measurements from *Chandra*, *XMM*, and *ROSAT* are potentially affected by the sensitivity varying across the field and must carefully address this systematic effect.

The other benefit of using the cross-correlation function with galaxies in the same field is one can sensitively probe the relative bias between AGN and galaxies as a function of their properties, and to first order cosmic variance will cancel in the relative bias. Cross-correlation functions provide accurate relative clustering measurements and do not introduce systematic effects; as shown in Coil et al. (2008), the relative bias inferred from cross-correlation measurements is consistent with that derived from the ratio of the auto-correlation functions. Recently, Hickox et al. (2009) measured the cross-correlation function of X-ray AGN with galaxies in the AGES survey (ref) at  $z = 0.5$  to infer an absolute bias of  $b = 1.34 \pm 0.16$  and a mean dark matter halo mass of  $\sim 1 \times 10^{13} h^{-1} M_\odot$ , similar to the results found here.

Several studies have investigated the dependence of X-ray AGN clustering on the hardness or hardness ratio of the source. Within the errors, we find no significant difference between AGN samples divided according to hardness ratio. Gilli et al. (2005) and Gilli et al. (2009) also find no significant difference in the clustering strength of soft and hard X-ray sources in the CDFN, CDFS, and COSMOS fields. Yang et al. (2003) detect a higher angular clustering signal for hard sources compared to soft sources, though without a well-known redshift distribution for the hard and soft samples this can not be interpreted as a significant difference in the intrinsic clustering properties. If, for example, the harder sources had a narrower redshift distribution, that would account for the different angular clustering signals.

We also find no significant dependence of clustering amplitude on X-ray luminosity within the range probed here. Plionis et al. (2008) claim to find a trend with brighter X-ray sources having higher clustering amplitudes, but these results rely on angular clustering measures without known redshift distributions, and the authors infer extremely large and implausible correlation lengths at  $z \sim 1$  of  $\sim 10 - 20 \text{ } h^{-1} \text{ Mpc}$ . Yang et al. (2006) detect a ‘weak’ correlation between clustering amplitude and X-ray luminosity when comparing their X-ray AGN clustering results with that of 2dF quasars (Croom et al. 2004), where X-ray luminosities for the quasars are estimated from their bolometric luminosities. They find that quasars are somewhat more clustered than X-ray AGN, though at  $< 2\sigma$  significance. This differs with what we find below (and the results shown in Figure 13), when comparing the clustering of X-ray AGN and quasars in the same volume at the same redshift. The  $z = 0.2$  results of Mullis et al. (2004) for brighter X-ray AGN do indicate a slightly higher correlation length than those at

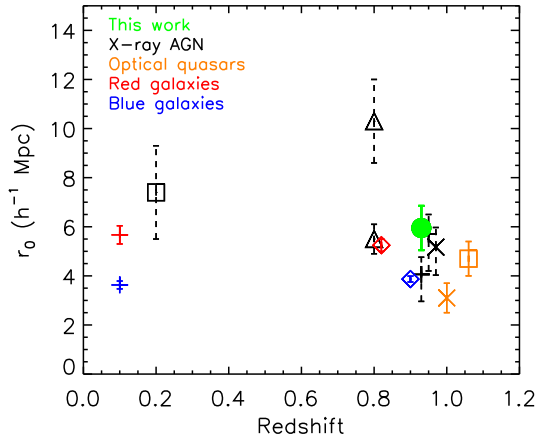


FIG. 13.— Clustering results for various AGN and galaxy surveys with  $0 < z < 1$ . The comoving correlation scale length,  $r_0$ , is plotted for different samples as a function of redshift. Shown in black with dashed line error bars are X-ray AGN clustering results from Mullis et al. (2004) (open box), Gilli et al. (2005) (triangle), Yang et al. (2006) (plus sign), and Gilli et al. (2009) (X sign). Results for X-ray AGN from this work are shown with a green filled circle. Results for red and blue galaxies are shown as red and blue markers for SDSS galaxies from Zehavi et al. (2005) (plus sign) and DEEP2 galaxies from Coil et al. (2008) (open diamond). At  $z = 0.1$  galaxy clustering results from 2dF are similar to those shown for SDSS. Orange markers indicate measures of optically-bright quasar clustering from Porciani, Magliocchetti, & Norberg (2004) (orange open box) and Coil et al. (2007) (orange X sign). The clustering of X-ray AGN found in this paper show that non-quasar X-ray AGN cluster similarly to red galaxies at  $z \sim 1$  and are more clustered than blue galaxies.

$z \sim 1$ , but that may be due to evolution and growth of structure, not intrinsic luminosity-dependent clustering.

The lack of a convincing relation between X-ray luminosity and clustering strength is important for theoretical models, as the X-ray luminosity is related to the black hole accretion rate for a fixed black hole mass. This may indicate then that there is not a strong correlation between accretion rate and host halo mass, i.e., between how much gas is accreted onto a black hole at a given time and how much gas potentially exists in the reservoir of the halo.

## 6.2. Comparison to Optical AGN Clustering Studies

A comparison of the clustering properties of different kinds of AGN can lead to a clearer understanding of their respective host galaxies, fueling mechanisms and AGN lifetimes. The clustering of X-ray AGN was not previously known to high enough precision to make a detailed comparison with other AGN samples. Among optically-selected AGN, clustering studies have been performed both for quasars at intermediate and high redshift and lower-luminosity Seyferts at low redshift.

Using the same techniques as here, Coil et al. (2007) find that spectroscopic broad-line SDSS quasars in the DEEP2 volume at  $0.7 < z < 1.4$  cluster like blue galaxies rather than red galaxies (at  $2\sigma$  significance), with  $r_0 = 3.1 \pm 0.6 h^{-1} \text{ Mpc}$ . Comparing the scale length found here for non-quasar X-ray AGN with that found by Coil et al. (2007) for quasars, the X-ray AGN are more clustered than quasars at the  $2.6\sigma$  level. This comparison should be quite robust, as the same sample of galaxies from the DEEP2 survey is used as a tracer of large-scale

structure in both analyses, and therefore the survey selection, and design are identical, as are the scales probed. This comparison suggests that high-accretion AGN, observed as optically bright quasars, are likely hosted in star-forming galaxies, while X-ray AGN are hosted both by massive blue galaxies and red galaxies, as seen in Figure 5 (see also Nandra et al. (2007)), reflecting a general correlation between the amount of star formation in a galaxy and the accretion rate of its central black hole (see e.g., Kauffmann et al. (2007) and Silverman et al. (2008) for other observational signatures of this general correlation). As both quasar fueling and star formation require the presence of cold gas, it is reasonable that they should be found in similar environments. If optically-bright, high-accretion quasars and lower-accretion X-ray AGN are similar objects at different evolutionary stages, then these results are consistent with a scenario in which a quasar resides in a star forming galaxy in the blue cloud before having its star formation quenched and moving to the red sequence with a lower luminosity X-ray AGN. The timescale between the quasar and lower-accretion X-ray AGN stages would have to be on the order of several Gyr, however, to allow enough time for the clustering amplitude to increase due to gravity.

Other studies of quasars at  $z \sim 1$  (e.g., Porciani, Magliocchetti, & Norberg 2004; Myers et al. 2006; da Ângela et al. 2005) find somewhat higher correlation lengths (consistent at the  $2\sigma$  level with the Coil et al. (2007) results) using the quasar auto-correlation function, though usually with larger error bars due to the low number density of quasars. The most constraining of these results is from Porciani, Magliocchetti, & Norberg (2004), using the 2QZ survey, who find  $r_0 = 4.7 \pm 0.7 h^{-1} \text{ Mpc}$  at  $z = 1.06$  (shown as an orange open box in Figure 13). This result is consistent with Coil et al. (2007) but allows a correlation length that matches either red or blue galaxies, given the error bars. This is generally true of other quasar clustering results at this redshift. Quasar clustering studies generally find a correlation slope,  $\gamma$ , of  $\sim 1.7$ , very similar to that of blue galaxies but lower than that of red galaxies at  $z \sim 1$  (Coil et al. 2008), which implies that quasars can not predominantly be hosted by red galaxies.

While a comparison of the quasar and AGN clustering results from DEEP2 point to AGN possibly being more clustered than quasars, a more precise measurement of the quasar clustering amplitude is needed to more firmly identify the host galaxy types and dark matter halo masses of quasars. The fundamental limitation in our ability to more precisely measure the quasar correlation function is the low number density of quasars; this makes cross-correlations of quasar samples with more abundant galaxy samples particularly effective. Future precise measurements of the quasar correlation function will likely come from wide-area galaxy redshift surveys at intermediate and high redshift.

## 6.3. Black Hole Masses for Quasars and X-ray AGN

The  $2\sigma$  difference in clustering amplitude measured at  $z \sim 1$  for quasars and X-ray AGN, if real, would reveal a difference in the mean host dark matter halo mass of these two populations, which could reflect a difference in the mean black hole masses for quasars and X-ray AGN. To investigate this we estimate black hole masses for the



quasars used in Coil et al. (2007) and the X-ray AGN used in this study.

To estimate black hole masses for the broad-line SDSS quasar population used in Coil et al. (2007), we use properties measured in the SDSS spectra, in particular the Mg II 2800 Å linewidth and UV flux, which are available for all of the quasars used in that study. The following estimator from McLure & Dunlop (2004) is used, which is calibrated at low redshift using reverberation mapping:

$$\frac{M_{BH}}{M_{\odot}} = 3.2 \left( \frac{\lambda L_{3000}}{10^{37} \text{W}} \right)^{0.62} \left[ \frac{\text{FWHM}(\text{MgII})}{\text{km s}^{-1}} \right]^2, \quad (8)$$

where  $L_{3000}$  is the restframe continuum luminosity at 3000 Å. We find that the SDSS quasars in the Coil et al. (2007) sample have a median black hole mass of  $M_{BH} = 3.0 \times 10^8 M_{\odot}$  and a mean mass of  $\overline{M}_{BH} = 4.3 \times 10^8 M_{\odot}$ , with a  $1\sigma$  standard deviation of  $3.4 \times 10^8 M_{\odot}$ , which agrees well with the masses of SDSS quasars at  $z \sim 1$  found by McLure & Dunlop (2004). There may be systematic biases associated with this method, particularly given that we are applying it at a different redshift than it was calibrated, but the estimated masses should be within a factor of  $\sim 2$ -3 of the true masses.

Black hole mass estimates for the X-ray AGN sample used in this paper are presented and discussed in Bundy et al. (2008), where the following relation between black hole mass and bulge infrared luminosity is used (Graham 2007):

$$\log \left( \frac{M_{BH}}{M_{\odot}} \right) = -0.37(M_{K_{\text{vega}}} + 24) + 8.29. \quad (9)$$

K-band photometry for the Chandra sources is from a Palomar/WIRC survey of the DEEP2 fields (Bundy et al. 2006). To estimate the black hole masses we assume no evolution in the black hole-bulge mass relation with redshift. We also assume that the host galaxies of the X-ray AGN are bulge-dominated and that the bulk of the K-band light is from the bulge. This is a reasonable assumption, as HST imaging shows that most of the X-ray AGN are in bulge-dominated galaxies (Pierce et al. 2007). There is a systematic effect, however, that would drive the black hole mass estimates lower as less of the K-band light is in the bulge. Here again we expect these black hole masses to be within a factor of  $\sim 2$ -3 of the true masses. We find that the median black hole mass for the X-ray AGN is  $M_{BH} = 4.7 \times 10^8 M_{\odot}$  and the mean is  $\overline{M}_{BH} = 6.2 \times 10^8 M_{\odot}$ , with a  $1\sigma$  standard deviation of  $5.8 \times 10^8 M_{\odot}$ .

The inferred X-ray AGN black hole masses are comparable to the quasar black hole masses, which could imply that they are in similar stellar mass galaxies. It may be surprising then if the non-quasar X-ray AGN are more clustered than the quasars. If true, this could indicate that quasars are more prevalent in lower mass halos because those halos have more fuel available to power the black hole.

Ferrarese (2002) finds a scaling between black hole mass and host dark matter halo mass at low redshift:

$$M_{BH}/10^8 M_{\odot} = 0.67 (M_{\text{halo}}/10^{12} M_{\odot})^{1.82}, \quad (10)$$

where results from Seljak (2002) have been used for halo profile fits derived from weak lensing measurements.

Given our rough black hole mass estimates above, this relation implies that both the SDSS quasars and non-quasar X-ray AGN should be in  $\sim 3 \times 10^{12} M_{\odot}$  halos, if there is no evolution in this relation to  $z \sim 1$ . As presented in Coil et al. (2008), from clustering measurements the minimum dark matter halo mass for blue galaxies at  $z \sim 1$  is  $M_{\text{min}} \sim 5 \times 10^{11} h^{-1} M_{\odot}$  and for red galaxies is  $M_{\text{min}} \sim 2 \times 10^{12} h^{-1} M_{\odot}$ . The corresponding mean halo masses for blue and red galaxies are  $\overline{M} \sim 1.8 \times 10^{12} M_{\odot}$  and  $\overline{M} \sim 5 \times 10^{13} M_{\odot}$ , respectively, for  $h = 0.7$ . Assuming that the scaling law between black hole mass and dark matter halo host mass does not evolve to  $z \sim 1$ , this would imply that quasars and non-quasar X-ray AGN reside either primarily in blue galaxies or in a mix of red and blue galaxies, which is consistent with the location of the X-ray AGN in the color-magnitude diagram.

#### 6.4. X-ray AGN and Green Galaxies

The clustering of ‘green’ galaxies in the minimum of the optical color bimodality at  $z \sim 1$  has been measured by Coil et al. (2008). A comparison of the green galaxies – which may be in transition from the blue, star forming galaxy population to the red, quiescent galaxy population – to our measurements for the X-ray AGN shows that both populations have a high clustering amplitude on large scales and therefore similar values of the correlation length ( $r_0 = 5.17 \pm 0.42 h^{-1}$  Mpc for green galaxies with  $M_B < -20$ ), comparable to red galaxies. Unlike red galaxies, however, green galaxies have a relatively shallow clustering slope,  $\gamma = 1.59 \pm 0.08$ , similar to that for blue, star-forming galaxies. The X-ray AGN clustering slope is not well constrained here and is consistent with the slope of either red or blue galaxies.

The location of the X-ray AGN in the optical color-magnitude diagram (see Figure 5) indicates that there is likely to be overlap between the X-ray AGN and green galaxy populations. Their clustering properties reinforce this; both populations reside in massive halos. The shallow slope of the green galaxy correlation function likely reflects a greater tendency for green galaxies to be found near the outskirts of dark matter halos, rather than their centers, compared to red galaxies. The same may be true for the X-ray AGN, though the apparent rise of  $w_p(r_p)$  on small scales might indicate that X-ray AGN are actually more likely to be central galaxies. However, given the large uncertainties in  $w_p(r_p)$  in the innermost bins we can not distinguish between these scenarios here.

#### 6.5. X-ray AGN in Groups

The higher clustering amplitude, found here at a significance of  $2.8 \sigma$ , for X-ray AGN compared to galaxies of the same color and magnitude distribution suggests that a higher fraction of X-ray AGN host galaxies are in groups than all galaxies of the same color and magnitude, as galaxies in groups have a higher clustering amplitude (Coil et al. 2006b; Yang et al. 2005). As discussed in Section 5.3, it can not be due to a difference in the stellar mass distribution of the AGN host galaxies compared to the matched galaxy sample, as they have similar stellar masses (as inferred from their host galaxy colors and luminosities). For a given massive galaxy sample, whether star forming or quiescent, it is the galaxies that reside in



more massive halos, and therefore are more likely to be in groups, that host X-ray AGN.

Georgakakis et al. (2008b) measure the fraction of X-ray AGN at  $z \sim 1$  in groups in AEGIS using the same *Chandra* and DEEP2 galaxy data used here. Using a DEEP2 group catalog (Gerke et al. 2005) that has been tested and calibrated with simulations and mock galaxy catalogs, they find that when compared to the full DEEP2 galaxy population X-ray AGN are preferentially found in groups, but when compared to galaxies of the same color and luminosity distribution of the AGN hosts this difference drops to the  $< 2\sigma$  level. This is almost certainly consistent with what we find here, as the higher clustering amplitude found for X-ray AGN host galaxies when compared to all galaxies of the same color and magnitude distribution does not imply that *all* X-ray AGN are in groups identified by Gerke et al. (2005), but rather that they generally reside in higher mass host halos which have a stronger likelihood of being in a group. Additionally, random errors are larger in the study of Georgakakis et al. (2008b), due to small number statistics for the group catalog, such that what is significantly detected here may be seen at lower significance in the group study.

#### 6.6. The Fueling of X-ray AGN

We find that non-QSO X-ray AGN host galaxies reside in more massive dark matter halos than the full population of galaxies of the same color and magnitude distribution. This likely reflects a higher incidence of X-ray AGN in galaxy groups than in isolated galaxies. Residing in a galaxy group may lead to accretion onto a central black hole, if galaxy mergers (which are more likely to occur in groups) generally supply gas to the central AGN (e.g., Barnes & Hernquist 1992; Mihos & Hernquist 1996; Springel, Di Matteo, & Hernquist 2005b). Alternatively, as X-ray AGN favor host dark matter halos that are on the massive end of the distribution for given observed galaxy properties, their presence in these halos may not reflect interactions with the environment, but rather a tendency for more massive black holes in otherwise similar galaxies to be found in more massive halos, possibly due to the presence of more gas that could fuel the black hole. For X-ray AGN in red host galaxies, there may be hot gas on large scales which could cool on small scales near the black hole to provide fuel.

The host galaxy morphologies of  $\sim 60$  X-ray AGN in AEGIS is studied by Pierce et al. (2007) (see also Georgakakis et al. in preparation), who find that roughly half of the host galaxies are elliptical or bulge-dominated, and that while the fraction that are classified as mergers is higher than for the field (at the  $2\sigma$  level), this accounts for only  $\sim 20\%$  of the population. It is therefore not clear that X-ray AGN are necessarily fueled by on-going or recent major mergers; they may be fueled by minor mergers or, in the case of those in red host galaxies, they may be fueled by small amounts of hot gas that remain long after a major merger. Indeed, roughly half of the X-ray AGN lie in red host galaxies that may have been on the red sequence for a long time and possibly not have undergone a major merger for many Gyr. To reconcile our results with a scenario in which X-ray AGN are fueled primarily by major mergers, one would require that those in red host galaxies had recently migrated to the red sequence (e.g.,

Salim et al. 2007; Schawinski et al. 2007; Shen et al. 2007; Georgakakis et al. 2008a; Kocevski et al. 2008).

As discussed above, the results presented here, when combined with those of Coil et al. (2007), are consistent with an evolutionary sequence in which bright quasars are ignited while being hosted by star forming galaxies and later evolve to be lower-luminosity AGN, detected in X-rays but not as broad-line optical sources, hosted by massive galaxies in either the bright or red end of the blue cloud or on the red sequence. This evolutionary sequence is not a unique explanation of the observations, i.e., X-ray AGN may be a different population than quasar relics, but if some fraction of blue star-forming galaxies have their star formation quenched and migrate to the red sequence, then it is plausible that some quasars may eventually become lower-luminosity AGN detected not by their optical light but by their X-ray emission. In this picture the AGN type could be due to gas availability in the host galaxy, which may be related to host halo mass (e.g., Croton et al. 2006; Dekel & Birnboim 2006).

The results presented here and in Coil et al. (2007) are generally consistent with the cartoon model shown in Hickox et al. (2009) for how galaxies and AGN evolve with time. In this cartoon model optically-bright quasars are hosted by on-going disk galaxy mergers and immediately precede an optically-faint X-ray AGN phase, which evolves into an early-type galaxy.

#### 6.7. Comparison to Theoretical Models of AGN Evolution

Theoretical models of AGN formation and evolution can yield measurably different predictions for the local environments and clustering properties of AGN. Kauffmann & Haehnelt (2002) use a semi-analytic model in which AGN are fueled by galaxy mergers, where the peak AGN luminosity depends on the mass of gas accreted by the black hole, which in turn depends on the host halo mass. This leads to a natural prediction that brighter AGN reside in more massive halos, such that the AGN clustering amplitude should be strongly luminosity-dependent. This model is not supported by observations, which generally show a lack of a strong correlation between AGN clustering amplitude and luminosity, except at the very bright end (e.g., Croom et al. 2002; Porciani & Norberg 2006; Myers et al. 2007; Shen et al. 2008).

Hopkins et al. (2005) present an alternative model in which bright and faint AGN are in similar physical systems but are in different stages of their life cycles. This model predicts that faint and bright AGN should reside in similar-mass dark matter halos and that quasar clustering should depend only weakly on luminosity (Lidz et al. 2006). That general prediction agrees well qualitatively with observations of quasar clustering, but the model also predicts that lower luminosity AGN should have an equal or lower clustering amplitude than bright AGN, which is not well-supported when comparing our results here for non-quasar X-ray AGN with the results for quasars in Coil et al. (2007). In the specific model presented by Hopkins et al. (2008), AGN are detected in X-rays while obscured by dust just after a major merger, before undergoing an optically-bright quasar phase a short time later; this picture is also not well-supported by our results.

The semi-analytic model of Croton et al. (2006) combines a prescription of merger-driven black hole growth similar to Kauffmann & Haehnelt (2000) with an independent mode for hot gas accretion in large halos which accounts for the fueling of lower-luminosity AGN in massive halos. This model assumes that some fraction of cold gas must be present to trigger a bright quasar phase during a galaxy merger; the black hole itself must also be massive such that the luminosity remains sub-Eddington. Quasars, in this model, can be strongly clustered at high redshift when cold gas fractions are presumably high, but as their host dark matter halos grow cooling becomes more inefficient as the virial temperature of the halo increases, and the cold gas supply is suppressed above a given threshold mass. Quasars will only be found in halos below the threshold mass, and thus relatively gas-free red galaxies are not expected to shine as quasars; only those mergers that occur in lower mass halos, presumably outside of group environments at  $z < 1$ , will contain sufficient cold gas to fuel a quasar. This model therefore predicts that quasars should cluster similarly to massive star-forming galaxies at a given redshift, where both the star formation and quasar activity are fueled by cold gas, while massive halos host lower-luminosity AGN that are fueled (possibly relatively inefficiently) by hot gas (which may cool on small scales near the black hole). X-ray AGN, in this picture, therefore should cluster like quasars did at an earlier epoch. There are no quantitative predictions from this model for the clustering of, say, the full X-ray AGN population versus bright quasars, but the model is qualitatively consistent with our results and the relatively higher clustering seen for quasars at high redshift (Myers et al. 2007; Shen et al. 2007; Croom et al. 2005).

Thacker et al. (2008) present a model for quasar fueling and feedback that quantitatively matches observations of quasar and X-ray clustering reasonably well. In their model bright AGN (both quasars and bright X-ray AGN) are the result of mergers and are augmented by feedback from AGN outflows. They do not present predictions for  $z < 1.2$ , but their model matches well the observed clustering of quasars at  $z = 1.5 - 2$ . Their prediction for the correlation length of X-ray AGN at  $z = 1.75$  with a luminosity  $L_X = 3.2 \times 10^{43} \text{ erg s}^{-1}$  is  $3.6 h^{-1} \text{ Mpc}$ , significantly lower than what we find here at  $z = 0.9$ . However, as it is not clear that the bulk of the X-ray AGN studied here are the result of major mergers, this model may not be entirely applicable to the results presented here.

## 7. CONCLUSIONS

Using the cross-correlation of galaxies and *Chandra*-detected AGN in the AEGIS survey, we are able to determine the clustering of X-ray AGN at  $z \sim 1$  much more precisely than studies that measure the clustering of AGN using the auto-correlation function of AGN alone. We find that non-quasar X-ray AGN with a median  $\log L_X \sim 43 \text{ erg s}^{-1}$  have a clustering scale length of  $r_0 = 5.95 \pm 0.90 h^{-1} \text{ Mpc}$  and slope of  $\gamma = 1.66 \pm 0.22$ , with a bias that corresponds to a minimum dark matter halo mass of  $M_{\min} = 5 (+5/-3) \times 10^{12} h^{-1} M_\odot$ . The clustering amplitude of X-ray AGN is consistent with that of red and ‘green’ galaxies at the same redshift and is

greater than that of blue galaxies, even though roughly half of the X-ray AGN are hosted by blue, star-forming galaxies. We do not find a significant difference in clustering amplitude within the AGN population when divided into subsamples based on optical luminosity, X-ray luminosity, or hardness ratio, within the ranges probed here.

The clustering strength of X-ray AGN is primarily determined by the host galaxy color; there is a smaller but significant effect due to a difference in clustering amplitude for galaxies that host X-ray AGN compared to matched samples of galaxies with the same color and luminosity distribution. This implies that galaxies that host X-ray AGN are in more massive dark matter halos than those that do not, for fixed host galaxy properties; i.e., galaxies that host X-ray AGN are more likely to be in groups when compared to galaxies of the same color and luminosity distribution.

By comparing to previous results on the clustering of optically-selected quasars in the DEEP2 fields, we find that non-quasar X-ray AGN are more clustered than optically-selected quasars at the same redshift at the  $2.6\sigma$  level. Our results are consistent with quasars occurring in blue star-forming galaxies which later settle onto the red sequence and potentially host lower-luminosity X-ray AGN, if they are similar objects at different evolutionary stages. While clustering measures of different types of AGN can be used to constrain their host galaxy types, halo masses, and fueling mechanisms, precise measurements await larger galaxy and AGN redshift surveys at intermediate and high redshift.

ALC would like to thank David Schlegel for measuring spectral quantities used to determine black hole masses for the SDSS quasars, Kevin Bundy for providing black hole mass estimates for the X-ray AGN, and Richard Cool for his help with the Hectospec data reduction. ALC would also like to thank Aaron Barth, Daniel Eisenstein, Jenny Greene, and Juna Kollmeier for useful discussions.

ALC was supported by NASA through Hubble Fellowship grant HF-01182.01-A, awarded by the Space Telescope Science Institute, which is operated by the Association of Universities for Research in Astronomy, Inc., for NASA, under contract NAS 5-26555. The DEEP2 team acknowledges support from NSF grants AST-0507483 and AST-0808133 and *Chandra* NASA grant GO8-9129A. The DEIMOS spectrograph was funded by a grant from CARA (Keck Observatory), an NSF Facilities and Infrastructure grant (AST92-2540), the Center for Particle Astrophysics and by gifts from Sun Microsystems and the Quantum Corporation. Much of the data presented herein were obtained at the W.M. Keck Observatory, which is operated as a scientific partnership among the California Institute of Technology, the University of California and the National Aeronautics and Space Administration. The Observatory was made possible by the generous financial support of the W.M. Keck Foundation. Additional observations reported here were obtained at the MMT Observatory, a joint facility of the University of Arizona and the Smithsonian Institution.

## REFERENCES

- Akylas, A., Georgantopoulos, I., & Plionis, M. 2000, MNRAS, 318, 1036
- Alexander, D. M., et al. 2001, AJ, 122, 2156
- Barger, A. J., et al. 2003, AJ, 126, 632
- Barnes, J. E., & Hernquist, L. 1992, ARA&A, 30, 705
- Basilakos, S., Georgakakis, A., Plionis, M., & Georgantopoulos, I. 2004, ApJ, 607, L79
- Basilakos, S., Plionis, M., Georgakakis, A., & Georgantopoulos, I. 2005, MNRAS, 356, 183
- Brandt, W. N., & Hasinger, G. 2005, ARA&A, 43, 827
- Bundy, K., et al. 2006, ApJ, 651, 120
- Bundy, K., et al. 2008, ApJ, 681, 931
- Cattaneo, A., et al. 2006, MNRAS, 370, 1651
- Coil, A. L., et al. 2004a, ApJ, 617, 765
- Coil, A. L., et al. 2004b, ApJ, 609, 525
- Coil, A. L., et al. 2006a, ApJ, 644, 671
- Coil, A. L., et al. 2006b, ApJ, 638, 668
- Coil, A. L., et al. 2007, ApJ, 654, 115
- Coil, A. L., et al. 2008, ApJ, 672, 153
- Comastri, A., & Fiore, F. 2004, Ap&SS, 294, 63
- Croom, S., et al. 2004, In ASP Conf. Ser. 311: AGN Physics with the Sloan Digital Sky Survey, p. 457
- Croom, S. M., et al. 2002, MNRAS, 335, 459
- Croom, S. M., et al. 2005, MNRAS, 356, 415
- Croton, D. J., et al. 2006, MNRAS, 365, 11
- da Ângela, J., et al. 2005, MNRAS, 360, 1040
- Davis, M., et al. 2003, Proc. SPIE, 4834, 161
- Davis, M., et al. 2007, ApJ, 660, L1
- Davis, M., & Peebles, P. J. E. 1983, ApJ, 267, 465
- Davis, M., Newman, J. A., Faber, S. M., & Phillips, A. C. 2000, In Proceedings of the ESO/ECF/STSCI Workshop on Deep Fields, Garching (Publ: Springer)
- Dekel, A., & Birnboim, Y. 2006, MNRAS, 368, 2
- Dekel, A., & Birnboim, Y. 2008, MNRAS, 383, 119
- Donley, J. L., et al. 2005, ApJ, 634, 169
- Faber, S., et al. 2003, Proc. SPIE, 4841, 1657
- Ferrarese, L. 2002, ApJ, 578, 90
- Ferrarese, L., & Ford, H. 2005, Space Science Reviews, 116, 523
- Ferrarese, L., & Merritt, D. 2000, ApJ, 539, L9
- Gebhardt, K., et al. 2000, ApJ, 539, L13
- Georgakakis, A., et al. 2007, ApJ, 660, L15
- Georgakakis, A., et al. 2008a, MNRAS, 385, 2049
- Georgakakis, A., et al. 2008b, MNRAS, p. 1197
- Gerke, B. F., et al. 2005, ApJ, 625, 6
- Gilli, R., et al. 2005, A&A, 430, 811
- Gilli, R., et al. 2009, Accepted to A&A
- Gilli, R., Comastri, A., & Hasinger, G. 2007, A&A, 463, 79
- Graham, A. W. 2007, MNRAS, 379, 711
- Heckman, T. M., et al. 2005, ApJ, 634, 161
- Hickox, R. C., et al. 2009, ApJ, 696, 891
- Hopkins, P. F., et al. 2005, ApJ, 625, L71
- Hopkins, P. F., & Hernquist, L. 2006, ApJS, 166, 1
- Hopkins, P. F., Hernquist, L., Cox, T. J., & Kereš, D. 2008, ApJS, 175, 356
- Kauffmann, G., et al. 2007, ApJS, 173, 357
- Kauffmann, G., & Haehnelt, M. 2000, MNRAS, 311, 576
- Kauffmann, G., & Haehnelt, M. G. 2002, MNRAS, 332, 529
- Kitzbichler, M. G., & White, S. D. M. 2007, MNRAS, 376, 2
- Kocevski, D. D., et al. 2008, arXiv:0809.2091
- Laird, E. S., et al. 2009, ApJS, 180, 102
- Lidz, A., Hopkins, P. F., Cox, T. J., Hernquist, L., & Robertson, B. 2006, ApJ, 641, 41
- Mainieri, V., et al. 2002, A&A, 393, 425
- McLure, R. J., & Dunlop, J. S. 2004, MNRAS, 352, 1390
- Mihos, J. C., & Hernquist, L. 1996, ApJ, 464, 641
- Miyaji, T., et al. 2007, ApJS, 172, 396
- Montero-Dorta, A. D., et al. 2008, MNRAS, p. 1355
- Morokuma, T., et al. 2008, ApJ, 676, 121
- Mullis, C. R., et al. 2004, ApJ, 617, 192
- Mushotzky, R. 2004, In Supermassive Black Holes in the Distant Universe, A. J. Barger, ed., volume 308 of *Astrophysics and Space Science Library*, p. 53
- Mushotzky, R. F., Cowie, L. L., Barger, A. J., & Arnaud, K. A. 2000, Nature, 404, 459
- Myers, A. D., et al. 2006, ApJ, 638, 622
- Myers, A. D., et al. 2007, ApJ, 658, 85
- Naab, T., et al. 2007, ApJ, 658, 710
- Nandra, K., et al. 2007, ApJ, 660, L11
- Peebles, P. J. E. 1980. The Large-Scale Structure of the Universe, Princeton, N.J., Princeton Univ. Press
- Pierce, C. M., et al. 2007, ApJ, 660, L19
- Plionis, M., et al. 2008, ApJ, 674, L5
- Porciani, C., & Norberg, P. 2006, MNRAS, 371, 1824
- Porciani, C., Magliocchetti, M., & Norberg, P. 2004, MNRAS, 355, 1010
- Richstone, D., et al. 1998, Nature, 395, A14
- Rovilos, E., & Georgantopoulos, I. 2007, A&A, 475, 115
- Salim, S., et al. 2007, ApJS, 173, 267
- Schawinski, K., et al. 2007, MNRAS, 382, 1415
- Seljak, U. 2002, MNRAS, 334, 797
- Shen, Y., et al. 2007, ApJ, 654, L115
- Shen, Y., et al. 2008, arXiv:0810.4144
- Silverman, J., et al. 2008, arXiv:0810.3653
- Smith, R. E., et al. 2003, MNRAS, 341, 1311
- Springel, V., Di Matteo, T., & Hernquist, L. 2005a, ApJ, 620, L79
- Springel, V., Di Matteo, T., & Hernquist, L. 2005b, MNRAS, 361, 776
- Thacker, R. J., Scannapieco, E., Couchman, H. M. P., & Richardson, M. 2008, arXiv:0811.2014
- Weiner, B. J., et al. 2009, ApJ, 692, 187
- Willmer, C., et al. 2006, ApJ, 647, 853
- Yang, X., Mo, H. J., van den Bosch, F. C., & Jing, Y. P. 2005, MNRAS, 357, 608
- Yang, Y., et al. 2003, ApJ, 585, L85
- Yang, Y., Mushotzky, R. F., Barger, A. J., & Cowie, L. L. 2006, ApJ, 645, 68
- Zehavi, I., et al. 2005, ApJ, 630, 1
- Zheng, Z., Coil, A. L., & Zehavi, I. 2007, ApJ, 667, 760